

1 **Experimental study of ~~non-Darcian flow~~non-Darcy flow characteristics in**
2 **permeable stones**

3
4
5 ~~A manuscript prepared for *Hydrology and Earth System Sciences*~~

6 ~~by~~

7 Zhongxia Li¹, Junwei Wan¹, Tao Xiong¹, Hongbin Zhan^{2*}, Linqing He³, Kun Huang^{1*}

8 ¹School of Environmental Studies, China University of Geosciences, 430074 Wuhan, China.

9 ²Department of Geology and Geophysics, Texas A & M University, College Station, TX
10 77843-3115, USA.

11 ³Changjiang Institute of Survey Technical Research MWR, Wuhan, China.

12 * ~~Corresponding~~ Correspondence to authors:

13 Dr. Hongbin Zhan (zhan@tamu.edu);

14 Dr. Kun Huang (cugdr_huang@cug.edu.cn).

15

16

17

18

19

20

21

22

23 **Abstract.**

24 This study provides experimental evidence of Forchheimer flow and transition between
25 different flow regimes from the perspective of pore size of permeable stone. ~~We have firstly~~
26 ~~carried out the seepage experiments of permeable stones with four different mesh sizes,~~
27 ~~including 24 mesh size, 46 mesh size, 60 mesh size, and 80 mesh size,~~ We have firstly carried
28 out the seepage experiments on four kinds of permeable stones with sizes of 24, 46, 60 and
29 80 mesh size, respectively, which corresponding to mean particle sizes (50% by weight) of
30 0.71 mm, 0.36 mm, 0.25 mm, and 0.18 mm. The seepage experiments show that obvious
31 deviation from ~~Darcian flow~~ Darcy flow regime is visible. In addition, the critical specific
32 discharge corresponding to the transition of flow regimes (from pre-~~Darcian~~ Darcy to post-
33 ~~Darcian~~ Darcy) increases with the increase of particle sizes. When the “pseudo” hydraulic
34 conductivity (K) (which is computed by the ratio of specific discharge (q) and ~~the~~ hydraulic
35 gradient) increases with the increase of ~~specific discharge (q),~~ the flow regime is denoted as
36 the pre-~~Darcian flow~~ Darcy flow. After ~~q the specific discharge~~ increases to a certain value, the
37 “pseudo” hydraulic conductivity begins to decrease, ~~and~~ this regime is called the post-
38 ~~Darcian flow~~ Darcy flow. In addition, we use the mercury injection ~~experiment technique~~ to
39 measure the pore size distribution of four permeable stones with different particle sizes, ~~and~~
40 ~~The~~ mercury injection curve is divided into three stages. The beginning and end segments of
41 the mercury injection curve are very gentle with relatively small slopes, while the
42 intermediate mercury injection curve is steep, indicating that the pore size in permeable
43 stones is relatively uniform. The porosity decreases as the mean particle sizes increases, ~~and~~
44 ~~The~~ mean pore size can faithfully reflect the influence of particle diameter, sorting degree
45 and arrangement mode of porous medium on seepage parameters. This study shows that the
46 size of pores is an essential factor for determining the flow regimes. In addition, the
47 Forchheimer coefficients are also discussed in which the coefficient A (which is related to the

48 linear term of the Forchheimer equation) is linearly related to $1/d^2$ as
49 $A = 0.0025(1/d^2) + 0.003$; while the coefficient B (which is related to the quadratic term of
50 the Forchheimer equation) is a quadratic function of $1/d$ as
51 $B = 1.14 \times 10^{-6} (1/d)^2 - 1.26 \times 10^{-6} (1/d)$. The porosity (n) can be used to reveal the effect of
52 sorting degree and arrangement on seepage coefficient. ~~The A~~ larger porosity leads to smaller
53 coefficients A and B under the condition of the same particle size.

54 **Keywords:** permeable stone, mercury injection [technique](#)~~experiment~~, pore size, flow regime,
55 ~~non-Darcian flow~~[non-Darcy flow](#).

56 1. Introduction

57 [Darcy \(1857\)](#) conducted a steady-state flow experiment in porous media and concluded
58 that ~~the~~ specific discharge was proportional to ~~the~~ hydraulic gradient, which is the Darcy's
59 law described as follow:

$$q = KJ \quad (1-1)$$

60 where q is the specific discharge, J is the hydraulic gradient, ~~and~~ K is the hydraulic
61 conductivity. However, when the specific discharge increases above a certain threshold,
62 deviation from Darcy's law is evident and the flow regime changes from ~~Darcian flow~~[Darcy](#)
63 [flow](#) regime to the so called ~~non-Darcian flow~~[non-Darcy flow](#) regime ([Bear, 1972](#)), which
64 was first observed by [Forchheimer \(1901\)](#), who proposed a widely used ~~non-Darcian~~
65 ~~flow~~[non-Darcy flow](#) equation (the Forchheimer equation) as follow:

$$J = Aq + Bq^2 \quad (1-2)$$

66 where A and B are constants related to fluid properties and pore structure. The first and
67 second terms on the right side of Eq. (1-2) ~~roughly more or less~~ reflect the contributions of

68 viscous and inertial forces (or resistance to flow), respectively.

69 From the Forchheimer equation, we can see that when the specific discharge is
70 sufficiently small, the inertial force can be ignored, ~~and~~ the equation is transformed to the
71 form of Darcy's law. On the other hand, when the specific discharge is sufficiently large, the
72 viscous force can be ignored, ~~and~~ the equation is transformed to the fully developed turbulent
73 flow.

74 In addition to the polynomial function such as the Forchheimer equation, there are also
75 several power-law functions proposed to describe the ~~non-Darcian flow~~non-Darcy flow, ~~and~~
76 one of the most commonly used power-law equations is the Izbash equation ([Izbash, 1931](#)),
77 which is written as:

$$J = aq^b \quad (4-3)$$

78 where a and b are the empirical parameters that depend on flow and materials properties, ~~and~~
79 the coefficient b is usually between 1 and 2.

80 Because of its applicability for a wide range of velocity spectrum and its sound physics,
81 many scholars have adopted the Forchheimer equation (among many different types of
82 equations) to explore the ~~non-Darcian flow~~non-Darcy flow. Besides, the theoretical
83 background of the Forchheimer equation has been discussed in details ([Panfilov and Fourar,](#)
84 [2006](#)). Numerous experimental data have confirmed the validity of the Forchheimer equation
85 for a variety of nonlinear flow phenomena ([Geertsma, 1974](#); [Scheidegger, 1957](#); [Wright,](#)
86 [1968](#)). The quadratic Forchheimer law has also been revealed as a result of numerical
87 modelling by simulating the Navier–Stokes flow in corrugated channels ([Koch and Ladd,](#)
88 [1996](#); [Skjetne et al., 1999](#); [Souto and Moyne, 1997](#)). To sum up, the Forchheimer equation
89 will be selected as a representative to describe non-Darcy flow in this study.

90 Since the transition between ~~Darcian flow~~Darcy flow and ~~non-Darcian flow~~non-Darcy

91 [flow](#) is important and difficult to quantify, different scholars have carried out experiments
92 using a wide range of porous media, including homogeneous and heterogeneous porous
93 media. Most of the experimental studies have focused on the influence of mean particle size
94 on flow state transition using homogeneous porous media. In fact, it was believed that the
95 nonlinear (or non-DarcianDarcy) flow behavior in porous media was due to turbulent effect
96 of flow in earlier studies and the Reynold number (Re) was widely used to quantify the
97 initiation of ~~non-Darcian flow~~[non-Darcy flow](#). [Bear \(1972\)](#) concluded that the critical Re
98 (denoted as Re_c) of flow states (or the Re value at which flow starts to change from Darcian
99 ~~flow~~[Darcy flow](#) regime to ~~non-Darcian flow~~[non-Darcy flow](#) regime) is between 1 to 10. This
100 finding was based on experimental data collected in packed sand beds ([Ergun, 1952](#); [Fancher](#)
101 [and Lewis, 1933](#); [Lindquist, 1933](#); [Scheidegger, 1960](#)). [Schneebeli \(1955\)](#) and [Wright \(1968\)](#)
102 experimentally measured the value of Re at the beginning of turbulence and concluded that at
103 very high velocities, the deviation from Darcy's law is due to inertial effects followed by
104 turbulent effects. In addition, [Dudgeon \(1966\)](#) confirmed that Re_c is about 60~150 for
105 relatively coarse particle medium including river gravels, crushed rock particles and glass
106 marbles with grain sizes from 16 mm to 152 mm. [Dudgeon \(1966\)](#) indicated that the
107 deviation from Darcy's law was not entirely due to turbulence, but in a large extent due to
108 inertial forces. Besides, [Geertsma \(1974\)](#) proposed an empirical relationship among the
109 inertial coefficient, permeability and porosity by conducting ~~non-Darcian flow~~[non-Darcy](#)
110 [flow](#) experiments in unconsolidated and consolidated sands. The laser anemometry and flow
111 visualization studies of fluid flow in porous structures were used by [Dybbbs and Edwards](#)
112 [\(1984\)](#), ~~and~~ they observed the nonlinear behavior at Reynolds numbers around 150. [Latifi et](#)
113 [al. \(1989\)](#) found that the transition from unsteady-state laminar flow to ~~non-Darcian flow~~[non-](#)
114 [Darcy flow](#) in packed beds of spheres was between Re values of 110 and 370. [Seguin et al.](#)
115 [\(1998\)](#) investigated the characterization of flow regimes in various porous media with

116 electrochemical techniques and found that the end of the ~~Darcian flow~~Darcy flow regime in
117 packed beds of particles appeared at Re about 180. Besides, [Bu et al. \(2014\)](#) indicated that the
118 ~~Darcian flow~~Darcy flow in the packed beds would end at Re around 100 by using
119 electrochemical techniques. [Sedghi-Asl et al. \(2014\)](#) found that the Darcy's law was usually
120 not valid for rounded particle sizes greater than 2.8 mm, according to the experimental results
121 of flow in different sizes of rounded aggregates. Our previous experimental research ([Li et al.,](#)
122 [2017](#)) indicated that when the particle size was smaller than 2.8 mm, the flow state gradually
123 changed from the pre-Darcy flow to the post-Darcy flow when the specific discharge
124 increased. When the medium particle sizes get even larger, such as 4.5 mm, 6.39 mm, 12.84
125 mm, and 16 mm ([Moutsopoulos et al., 2009](#)), only the post-Darcy flow exists. Based on
126 above analysis, we can see that many previous experiments were carried out on homogeneous
127 porous media, ~~and~~ the non-Darcy flow characteristics are quite different in porous media with
128 various particle sizes.

129 Among the numerous experimental studies reviewed above on transition of Darcy flow
130 to non-Darcy flow~~this issue~~, it is evident that most of them focused on the effect of the mean
131 particle size rather than the particle size distribution. Recently, a few investigators recognized
132 the importance of particle size heterogeneity in understanding the transition of flow regimes,
133 and have carried out a series of experiments to address the issue. For instance, [Van Lopik et](#)
134 [al. \(2017\)](#) provided new experimental data on nonlinear flow behavior in various uniformly
135 graded granular material for 20 samples, ranging from medium sands ($d_{50} > 0.39$ mm) to
136 gravel ($d_{50} > 6.34$ mm). In addition, they investigated the nonlinear flow behavior through
137 packed beds of ~~5-five~~ different types of natural sand and gravel from unconsolidated aquifers,
138 as well as 13 different composite mixtures of uniformly graded filter sands at different grain
139 size distributions and porosity values ([Van Lopik et al., 2019](#)). We have also discussed the
140 effect of particle size distribution on Forchheimer flow and transition of flow regimes in a

141 previous study ([Li et al., 2019b](#)). ~~And~~ Our [previous](#) study showed that the uniformity
142 coefficient of porous media (a term used to describe the pore size distribution) is a critical
143 factor for determining the flow regimes besides the mean particle sizes. [Yang et al. \(2019\)](#)
144 investigated the effects of the particle size distribution on the seepage behavior of a sand
145 particle mixture ~~subjected~~ and evaluated the validity of empirical formulas of permeability
146 and inertia factor used in engineering practice. [Shi et al. \(2020\)](#) discussed the non-
147 ~~Dare~~[Darcy](#) flow behavior of granular limestone with a wide range of porosity from 0.242 to
148 0.449. Based on the experimental data, [Shi et al. \(2020\)](#) proposed an empirical hydraulic
149 conductivity-porosity relation as well as an expression of inertial coefficient. Regardless of
150 the media investigated are homogeneous or heterogeneous, the essence of the water passing
151 capacity of porous media is pore sizes. Thus, exploring the distribution of pores in porous
152 media is the basis of studying flow dynamics of [Darcyan](#) and ~~non-Darcian flow~~[non-Darcy](#)
153 [flows](#).

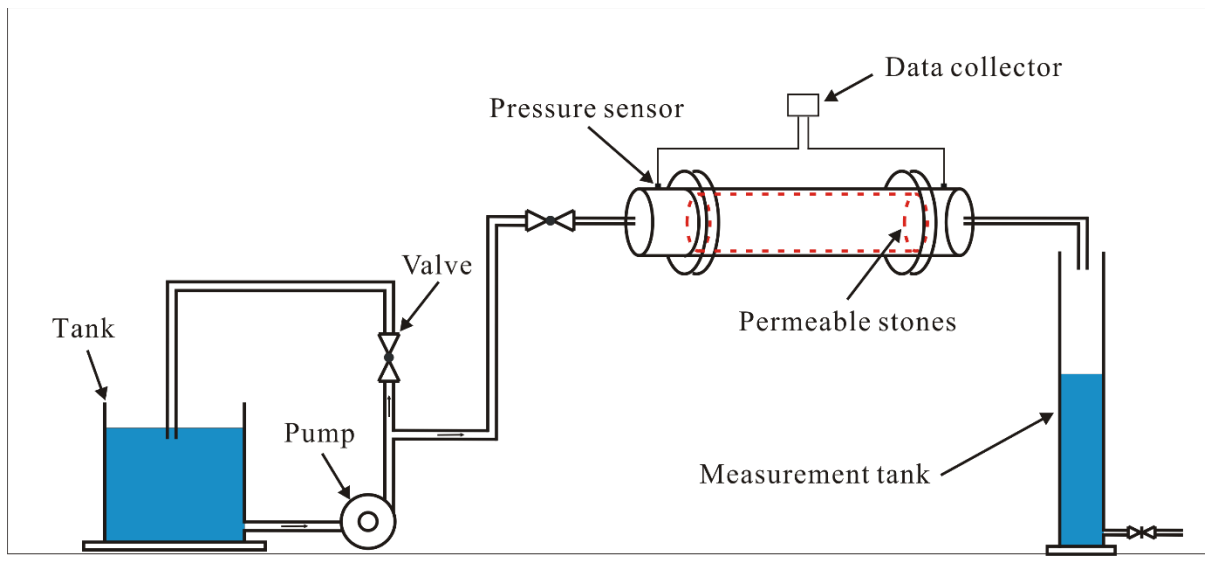
154 The purpose of this study is to provide a quantitative analysis on the effects of pore size
155 on the transition of flow regimes between [Darcyan](#) and ~~non-Darcian flow~~[non-Darcy flows](#)
156 based on a series of laboratory experiments. To meet the objectives, we have firstly carried
157 out the seepage experiments of permeable stones with four different particle sizes. After that,
158 we have conducted mercury injection experiments on permeable stones with four different
159 particle sizes, ~~and~~ the pore size distributions with different particle sizes are obtained. Finally,
160 the effect of pore size on the transition of flow regimes and Forchheimer coefficients are
161 discussed based on the experimental results.

162 **2. Experimental methodology**

163 **2.1 Experimental setup and methods**

164 The experimental device is mainly composed of three parts: a water supply device, a
165 seepage experimental device and a measuring device. The schematic diagram of the

166 experimental apparatus is shown in Fig. 1. The water supply device consists of a tank, a
167 centrifugal pump and a flow regulating valve. The seepage experimental device consists of a
168 permeable stone and a plexiglass column. The measurement device monitors the real-time
169 water temperature and pressure. The water temperature is measured using a thermometer with
170 a precision of measurement of 0.1 °C. The water-level fluctuation is measured to calculate the
171 flow rate by a pressure transducer (CY201, Chengdu test LLC, China) in the range of 0–20
172 kPa with $\pm 0.1\%$ accuracy. The measuring device consists of a cylindrical tank and a pressure
173 transducer. The sample of permeable stone is 60 mm in length with a circular cross section of
174 51.3 mm in diameter. Two pressure transducers are set at the entrance and exit of the column
175 to measure the pressure drop. To minimize the boundary effects, the pressure transducer is
176 placed 30 mm away from either end of the column, ~~and~~ the way of pressure measurement is
177 consistent with our previous studies ([Li et al., 2017](#); [Li et al., 2019b](#)).



179 Figure 1. The schematic diagram of experimental apparatus.

180 2.2 Experimental Materials and Procedures

181 Four different particle sizes of permeable stones are selected to carry out the seepage
182 experiment in this study. It is necessary to make a brief overview of the preparation process
183 of permeable stone, which is a type of artificially made tight porous medium formed by sand

184 grains and cementing compound. In the process of preparing permeable stonestones, a certain
185 particle size of sand and cementing compound is put in a mold, ~~and~~ which is consolidated at
186 room temperature. The permeable stone is widely used in daily life. At present, the most
187 commonly used permeable base materials in urban road construction, “sponge” city
188 construction and ecological restoration research are large-pore cement stabilized gravel,
189 large-diameter permeable asphalt mixture and so on (Guan et al., 2021; Li et al., 2019a; Suo
190 et al., 2021; Yu et al., 2021). ~~Permeable stone is widely used in urban road design, sponge~~
191 ~~city construction and ecological effect research (Guan et al., 2021; Li et al., 2019a; Yu et al.,~~
192 ~~2021).~~ ~~And the most commonly used permeable base materials are large pore cement~~
193 ~~stabilized macadam, large diameter permeable asphalt mixture and so on (Suo et al., 2021).~~
194 The discharge capacity of various permeable stones is different. For permeable stone, there
195 ~~must be a certain connected pore space to maintain a certain permeability for transmitting~~
196 ~~water.~~ However, the increase of pore space will lead to the decrease of pavement performance
197 and mechanical strength (Han et al., 2016; Wang et al., 2021). Therefore, many scholars have
198 carried out a lot of research on controlling the proper pore space of permeable stone (Alvarez
199 et al., 2010; Prowell et al., 2002; Xie and Watson, 2004).

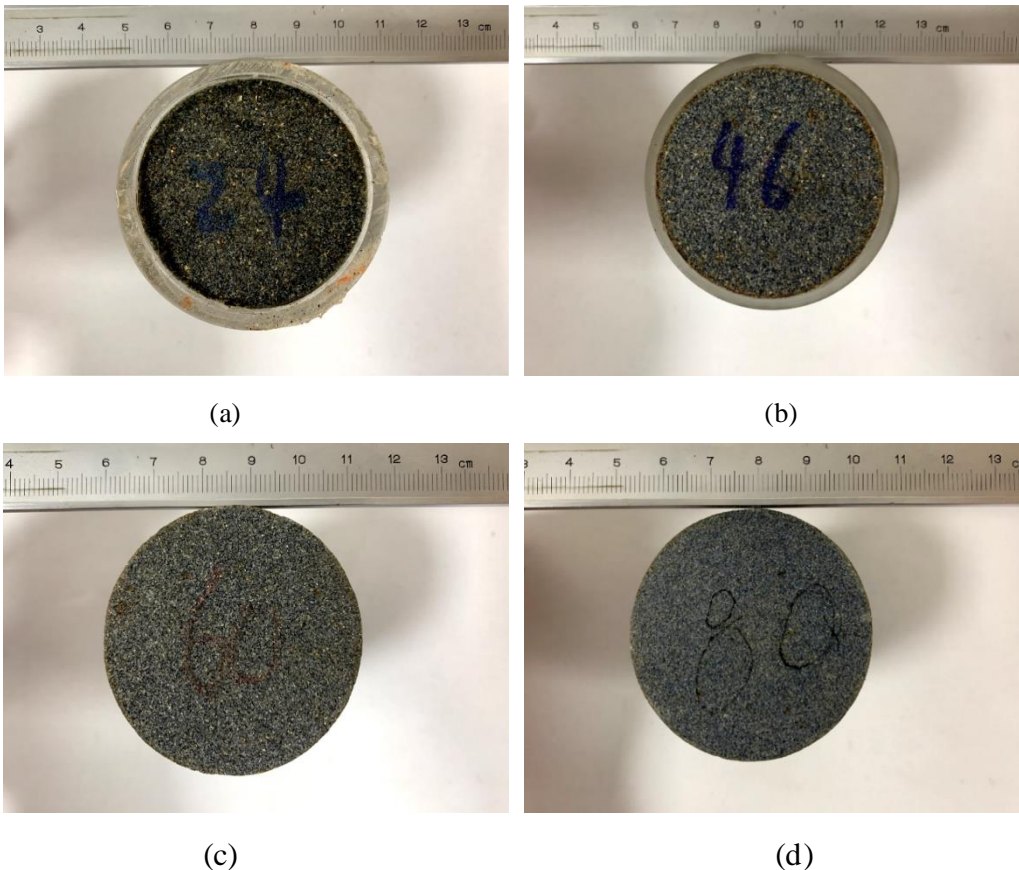
200 We have carried out the seepage experiments on four kinds of permeable stones with
201 different sizes of 24, 46, 60 and 80 mesh size,~~of permeable stones with four different mesh~~
202 ~~sizes, including 24 mesh size, 46 mesh size, 60 mesh size, and 80 mesh size, and~~ where the
203 mesh size is defined as the number of mesh elements (all in square shapes) in a one inch by
204 one inch square, which means that ~~thus~~ a greater number of mesh size implies a smaller
205 particle size. For instance, we can convert above four different mesh sizes of permeable
206 stones into corresponding particle sizes of 0.71 mm, 0.36 mm, 0.25 mm and 0.18 mm,
207 respectively. In respect to pore composition, the pore distribution is concentrated over a
208 narrow pore size range, the proportion of large pores and small pores is very small. The

209 average particle size can reflect the overall permeability of the porous media. The pore
210 structure of permeable rock will not change in the process of the seepage experiment under
211 room temperature, ~~and~~ the physical diagrams of four kinds of permeable stones with different
212 particle sizes are shown in Fig. 2 and Fig. 3.



213

214 Figure 2. Physical drawing of permeable stones with four different particle sizes.



215

216

217

218

219 Figure 3. Permeable stones with different particle sizes: (a) 24 mesh size or 0.71 mm, (b) 46

220 mesh size or 0.36 mm, (c) 60 mesh size or 0.25 mm, and (d) 80 mesh size or 0.18 mm.

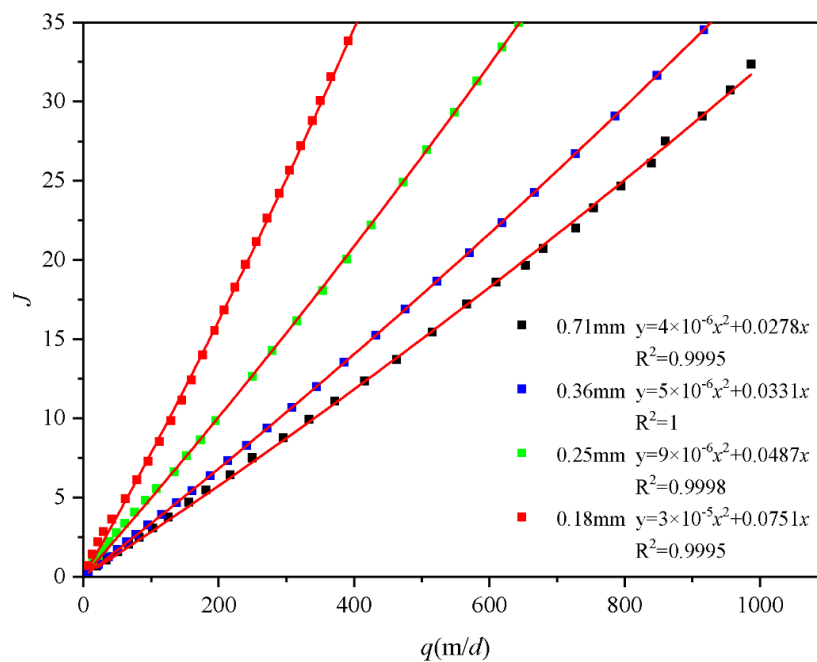
221 It is worth mentioning that the contact surface of the sample and the plexiglass column
222 is sealed to prevent any preferential flow through the wall of the plexiglass column. After the
223 permeable stone is inserted into the plexiglass column, both ends are sealed with silicone glue.
224 ~~The~~ Water passing through the permeable stone is then collected by a cylindrical tank.
225 Moreover, the ratio of the internal diameter of the column to the particle size of permeable
226 stone is greater than 12, which can eliminate any possible wall effect on the seepage
227 according to [Beavers et al. \(1972\)](#). When carrying out the experiment, it usually takes about
228 two hours to saturate the permeable stone. For each packed sample, more than 25 tests with
229 different constant inlet pressures were conducted under steady-state flow condition. In
230 addition, for each group of permeable stone, repeated tests under the same experimental
231 condition were carried out 3-4 times to ensure the accuracy of the results.

232 3. Results and discussion

233 3.1 Permeable stone seepage experiment

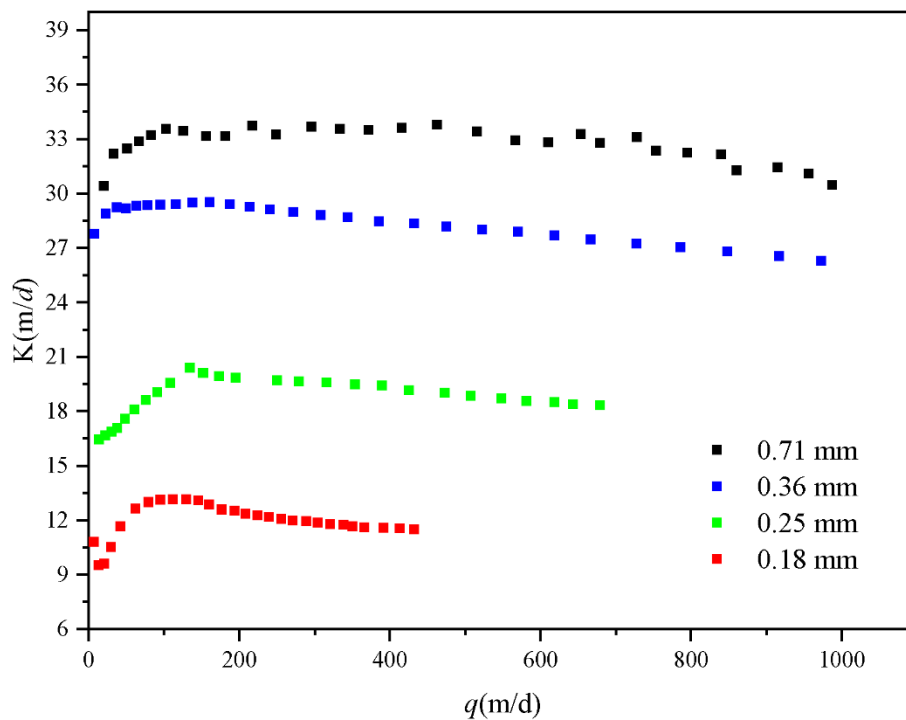
234 In this study, ~~we selected permeable stone with four different particle sizes as the~~
235 ~~research objects, including 24 mesh size, 46 mesh size, 60 mesh size and 80 mesh size. The~~
236 ~~mesh size is the number of holes per inch of screen mesh and the particle size is inversely~~
237 ~~proportional to the mesh size. The mean particle sizes corresponding to the four different~~
238 ~~mesh sizes are 0.71 mm, 0.36 mm, 0.25 mm, and 0.18 mm, respectively, where the mean~~
239 ~~particle size is corresponding to 50% by weight hereinafter~~ ~~in this study~~. Such a definition of
240 mean particle size may be different from some other studies such as [Fetter \(2001\)](#) which has
241 used 10% by weight as the mean particle size. The relationship between the specific
242 discharge (q) and the hydraulic gradient (J) of permeable stones is plotted in Fig. 4. The units
243 of specific discharge mentioned in this study are all converted to meters per day (m d^{-1}).
244 ~~To better compare with the actual groundwater flow, we converted the specific discharge to~~
245 ~~meters per day (m d^{-1}).~~ Therefore, the best-fitting exercise yields Forchheimer numbers

246 with orders of magnitudes to be about -4. In addition, the critical Forchheimer numbers
 247 proposed by [Zeng and Grigg \(2006\)](#) and [Javadi et al. \(2014\)](#) are empirical, ~~in~~ In fact, the
 248 transition between Darcy to non-Darcy is successional over a certain range of Forchheimer
 249 numbers. The ~~non-Darcian flow~~ non-Darcy flow criterion applicable to different pore media is
 250 established by conducting seepage resistance experiments in homogeneous and
 251 heterogeneous porous media in our previous study ([Li et al., 2017](#); [Li et al., 2019b](#)), which is
 252 consistent with the results of [Zeng and Grigg \(2006\)](#). Generally speaking, the q - J and q - K
 253 curves are the most commonly used methods to analyze flow regime when conducting
 254 seepage resistance experiments in porous media. However, the nonlinear characteristics of q -
 255 J curve are not obvious due to the relatively small velocity range used in the experiments.
 256 The traditional hydraulic conductivity is the ratio of the specific discharge versus the
 257 hydraulic gradient (q/J), ~~and~~ it is a constant if Darcy's law is applicable, which is denoted as
 258 K_D ([Li et al., 2019b](#)). In fact, the ratio of q/J is no longer a constant for the problems
 259 discussed in this study. In a word, the q - K curve can be used to observe the transition of flow
 260 state more intuitively.



262 Figure 4. Variation of J with q of four permeable stones with different particle sizes.

263 Fig. 4 shows that when q is somewhat the same, a larger mesh size (which means a
 264 smaller particle size) will lead to a larger J . And the results are consistent with our previous
 265 studies (Huang et al., 2013; Li et al., 2017; Li et al., 2019b). However, the nonlinear
 266 characteristics of q - J curve are not obvious due to the relatively small velocity range used in
 267 the experiments. Nevertheless, the best-fitting results using the Forchheimer equation are
 268 satisfactory. To analyze the influence of pore size on seepage flow regimes, we have obtained
 269 the relationship between q and the "pseudo" hydraulic conductivity (K) (which is computed
 270 using q/J) of four permeable stones with different particle sizes, as shown in Fig. 5. We
 271 should point out that the "pseudo" hydraulic conductivity term discussed here for ~~non-~~
 272 ~~Darcian flow~~non-Darcy flow is usually not a constant, thus it is different from the hydraulic
 273 conductivity term used in Darcy's law, which is a constant. It is obvious that the hydraulic
 274 conductivity is not a constant with the increase of specific discharge, so it is called the
 275 "pseudo" hydraulic conductivity (Li et al., 2019b).



276
 277 Figure 5. Variation of K with q of four permeable stones with different particle sizes.

278 We can divide the q - K curve into two segments: for the first segment, K increases with

279 the increase of q , which is denoted as the pre-~~Darcian flow~~Darcy flow. For the second
280 segment, after q increases to a certain value, K begins to decrease with q , which is called the
281 post-~~Darcian flow~~Darcy flow. In fact, [Izbash \(1931\)](#) presented the equation as
282 $q = M \left(\frac{dH}{dx} \right)^m = Mi^m$, where M and m are the coefficients determined by fluid flow and
283 properties of porous media. When $m=1$, the Izbash equation reduces to Darcy law, when $m>1$,
284 the Izbash equation corresponds to the pre-Darcy~~y~~ flow and when $m<1$, the Izbash equation
285 refers to the post-Darcy~~y~~ flow ([Dejam et al., 2017](#); [Soni et al., 1978](#)). Besides, [Dejam et al.](#)
286 [\(2017\)](#) carried out a more detailed study on issues related to the pre-Darcy and post-Darcy
287 flows. ~~And t~~The influence of pre-Darcy flow on the pressure diffusion for homogenous
288 porous media is studied in terms of the nonlinear exponent and the threshold pressure
289 gradient. When the hydraulic gradient is small (and q is small as well), a great portion of
290 water is bounded (or becomes immobile) on the surface of solids due to the solid-liquid
291 interfacial force, ~~and~~ only a small fraction of the water is mobile and free to flow through the
292 pores. In addition, another justification for the pre-Darcy behavior may be due to an effect of
293 a stream potential which generates small countercurrents along pore walls in a direction
294 ~~against opposite that of~~ the main flow ([Bear, 1972](#); [Scheidegger, 2020](#)). ~~And~~ [Swartzendruber](#)
295 [\(1962b\)](#) stated that the surface forces arose in a solid-fluid interface due to strong negative
296 charges on clay particle surfaces, and the dipolar nature of water molecules caused a pressure
297 gradient response to be nonlinear and led to the pre-Darcy flow ([Swartzendruber, 1962a](#)). As
298 the hydraulic gradient increases (and q increases as well), the initial threshold for mobilizing
299 the previously immobile water near the solid-liquid surface is overcome and more water
300 participates in ~~the~~ flow. For this reason, the "pseudo" hydraulic conductivity increases with
301 the increase of hydraulic gradient and the specific discharge in the first segment. When the
302 specific discharge increases to the critical specific discharge (q_c), the "pseudo" hydraulic

303 conductivity is maximized. According to $K = \frac{q}{Aq + Bq^2} = \frac{1}{A + Bq}$ based on Eq. (4-2), we can
304 find that the "pseudo" hydraulic conductivity begins to decrease as the specific discharge
305 continues to increase. Besides, the critical specific discharge corresponding to the transition
306 of flow regimes (from pre-DarcianDarcy to post-DarcianDarcy) increases with the increase of
307 particle sizes (or decrease of mesh sizes).

308 3.2 Mercury injection experiment

309 The particle size, different grain size distributions and degree of sorting are the main
310 factors that determine the size and shape of pores. ~~And~~ The shape of the pores determines
311 the tortuosity and distribution of flow paths, which are related to viscous and inertial flow
312 resistances. It is generally accepted in previous studies that the pore sizes of porous media
313 have an impact on the seepage law ([Maalal et al., 2021](#); [Zhou et al., 2019](#)). However, the
314 structure of natural porous media is very complex, and it is difficult to quantify the effects of
315 the arrangement of particles on the seepage law. The characteristics of pore size distribution
316 contains critical information for quantifying the flow regimes. The mercury intrusion
317 porosimetry and the nitrogen adsorption isotherm are two commonly used methods to
318 characterize the pore sizes and their distribution ([Rijfkogel et al., 2019](#)). Besides, other
319 techniques can also be used to derive the pore size distribution, such as small-angle neutron
320 and X-ray scattering measurements, CT images and nuclear magnetic resonance ([Anovitz and](#)
321 [Cole, 2015](#); [Hall et al., 1986](#); [Kate and Gokhale, 2006](#); [Lindquist et al., 2000](#)). In this study
322 we will use the mercury injection ~~technique~~ experiment to measure the pore size distribution
323 of the four permeable stones with different particle sizes and use the information to describe
324 the flow regimes.

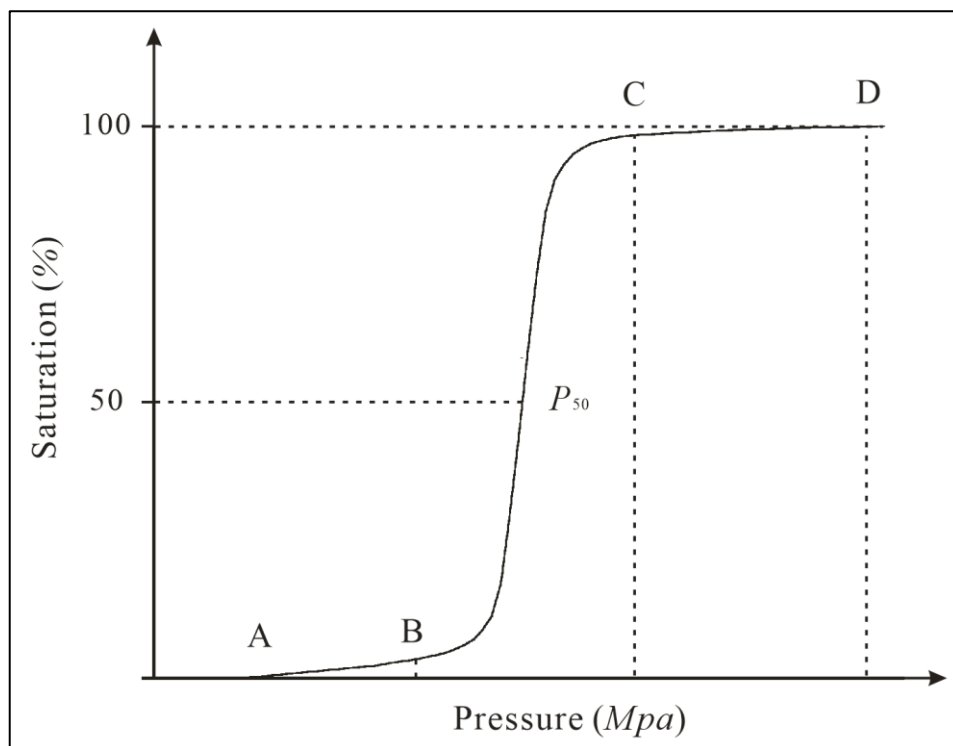
325 To quantitatively study the pore size and pore throat distribution, we need to envisage a
326 physically based conceptual model to describe the pore structures of permeable stones. The

327 commonly used model is the so-called capillary model ([Pittman, 1992](#); [Rezaee et al., 2012](#);
 328 [Schmitt et al., 2013](#)), which approximates the connected pores as many paralleled capillaries.
 329 ~~And~~ The capillary forces are generated at the phase interface due to the surface tension
 330 between the solid and liquid phases when liquid flows in a capillary. The capillary force is
 331 directed toward the concave liquid level, ~~and~~ it is shown as ([Washburn, 1921](#)):

$$P_c = \frac{2\sigma \cos \theta}{r} \quad (3-14)$$

332 where P_c is the capillary force, σ is the solid-liquid interfacial tension, θ is the wet angle
 333 between the liquid and the solid surface, ~~and~~ r is the radius of curvature in capillary.

334 Since mercury is a nonwetting phase to solids, so to get mercury into the pores of the
 335 permeable stone, an external force (or displacement pressure) must be applied to overcome
 336 the capillary force. When a greater pressure is applied, mercury can enter smaller pores.
 337 When a certain pressure is applied, the injection pressure is equivalent to the capillary
 338 pressure in the corresponding pore. Then we can calculate the corresponding capillary radius
 339 according to Eq. (3-14), ~~and~~ the volume of mercury injected is the pore volume.



340

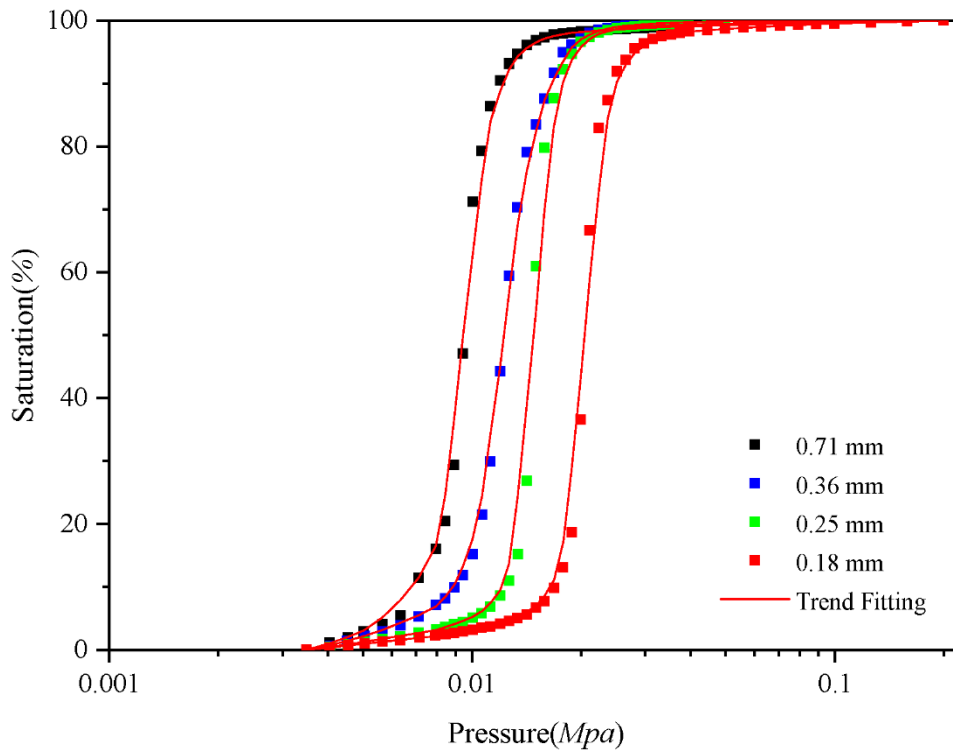
341 Figure 6. Schematic diagram of pressure changes with saturation: the initial stage (A-B), the
342 intermediate mercury entry stage (B-C), and the end stage (C-D).

343 By continuously increasing the injection pressure, one can obtain the curve of injection
344 pressure and the volume of injected mercury, from which one can also obtain the pore-throat
345 distribution curve and capillary pressure curve. According to the amount of mercury injected
346 at different injection pressures, the relation between the injection pressure and the injection
347 saturation is shown in Fig. 6.

348 Fig. 6 shows that the mercury injection curve can be divided into three stages. Firstly,
349 during the initial stage (A-B) which has a very mild slope, the intake pressure is very small
350 and the intake saturation is also very low. With the increasing of the injection pressure, the
351 intake saturation slowly increases. Secondly, during the intermediate mercury entry stage (B-
352 C) which has a steep slope, a small pressure change will lead to a significant saturation
353 change. This means that the pores are relatively uniform and the differences in pore sizes are
354 small. It is well known that for mercury injection experiments, as injection pressure increases,
355 the injection saturation will gradually increase and eventually all the pores will be filled with
356 mercury. As can be seen from Fig. 7, with the continuous injection of mercury, the pressure of
357 permeable stones with different particle sizes varies with saturation, which is reflected in the
358 different pressures P_B and P_C at different stages. However, the reason for observing the
359 different pressures s is the difference of pore size distribution in the permeable stones.
360 Therefore, the pressure ratio of B and C (P_C/P_B) can be used as one of the criteria to
361 characterize the heterogeneity of pore size in porous media. Besides, when the saturation
362 reaches 50%, the corresponding pressure value (P_{50}) reflects the characteristics of the mean
363 pore size, ~~and~~ a larger P_{50} leads to a larger mean pore size. Finally, during the end stage (C-D)
364 which has a very mild slope as well, the amount of mercury will not increase considerably
365 when the injection pressure increases. This indicates that nearly all the pores are essentially

366 filled with mercury, ~~and~~ then the mercury injection experiment is completed. After
367 completing the mercury injection experiments, we have obtained the mercury injection curves
368 of four permeable stones with different particle sizes, as shown in Fig. 7.

369 We can make a number of interesting observations based on Fig. 7. Firstly, the pressure
370 at the starting point (when the saturation begins to increase), denoted as P_A , increases as the
371 mean particle size decreases. This means that the maximum pore size in permeable stone
372 decreases with the decrease of the mean particle sizes. Secondly, the mercury injection curves
373 of four permeable stones all include steep intermediate stages, indicating that the pore size
374 distributions are all relatively uniform. ~~And~~ The corresponding pressure values at points B
375 and C increase as the mean particle sizes decrease. Moreover, the pressure ratios
376 corresponding to points B and C (P_C/P_B) also decrease with the decrease of particle sizes,
377 suggesting even more uniform pore size distributions with decreasing particle sizes. Thirdly,
378 the intermediate mercury entry stages gradually shift to the right with the decrease of particle
379 sizes. When the saturation reaches 50%, the corresponding pressure (the median pressure)
380 decreases with the increase of the mean particle sizes. Fourthly, the mercury injection curves
381 of these four permeable stones with different particle sizes all approach 100% saturation with
382 very mild slopes, indicating that there are few small pores in the permeable stones. We have
383 extracted the key pressure characteristic values of mercury injection experiment of Fig. 7, and
384 listed the results in Table 1.



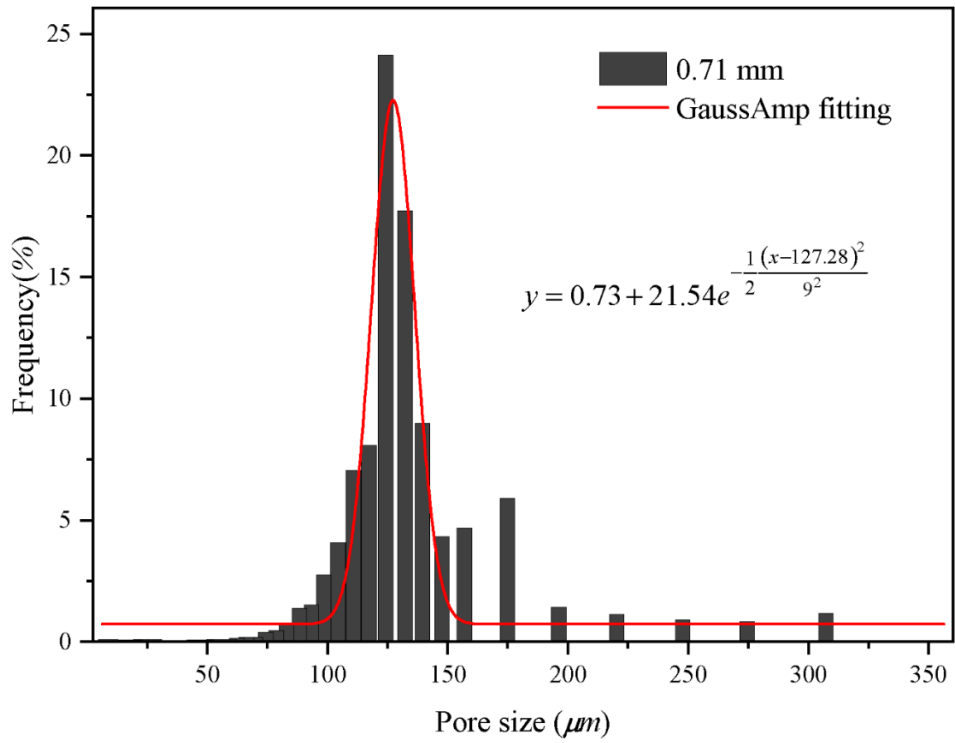
385

386 Figure 7. Variation of pressure with saturation of four permeable stones with different particle
 387 sizes.

388 Table 1. Pressure characteristic values of four permeable stones with different particle sizes.

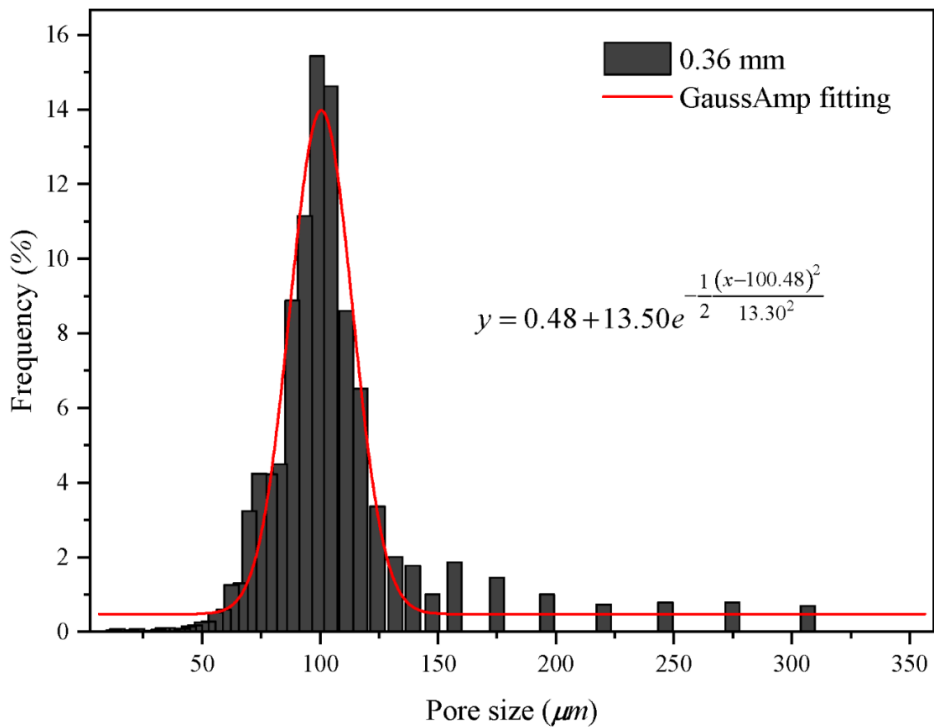
Mesh size	$P_A(MPa)$	$P_B(MPa)$	$P_C(MPa)$	$P_{50}(MPa)$	P_C/P_B
24	0.0041	0.0064	0.0133	0.0094	2.0987
46	0.0045	0.0071	0.0188	0.0119	2.6374
60	0.0051	0.0112	0.0211	0.0150	1.8764
80	0.0057	0.0158	0.0281	0.0211	1.7758

389 To observe the pore size distributions of the four permeable stones with different particle
 390 sizes in more details, we can calculate the percentages of different pore sizes in permeable
 391 stones according to the mercury injection curves, as shown in Figs. 8-11.



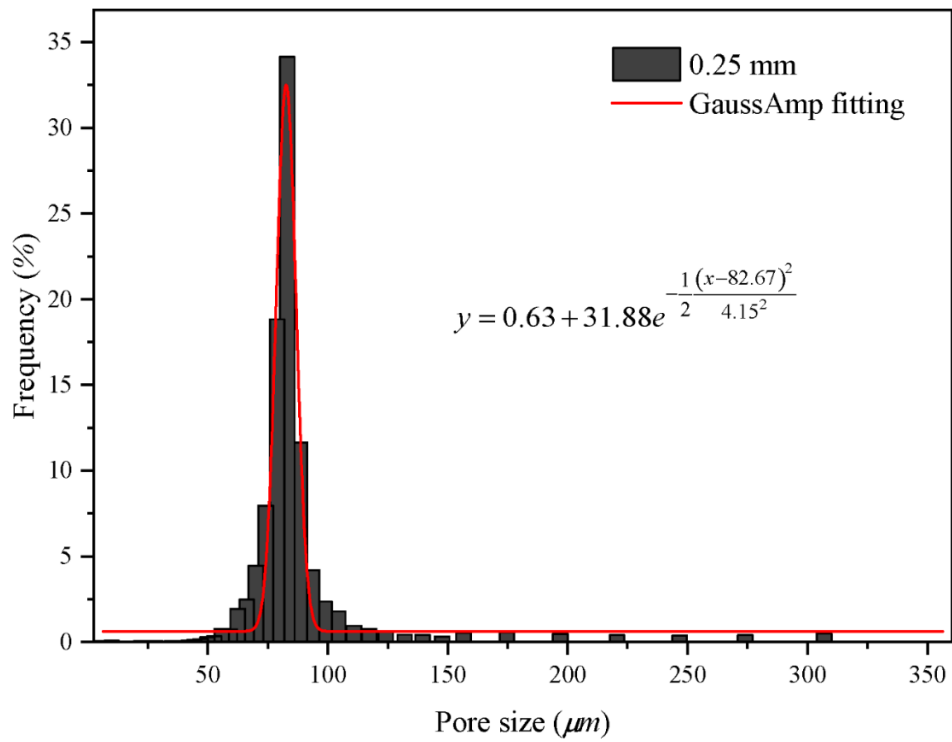
392

393 Figure 8. Histogram of pore size distribution of permeable stone with diameter of 0.71 mm.



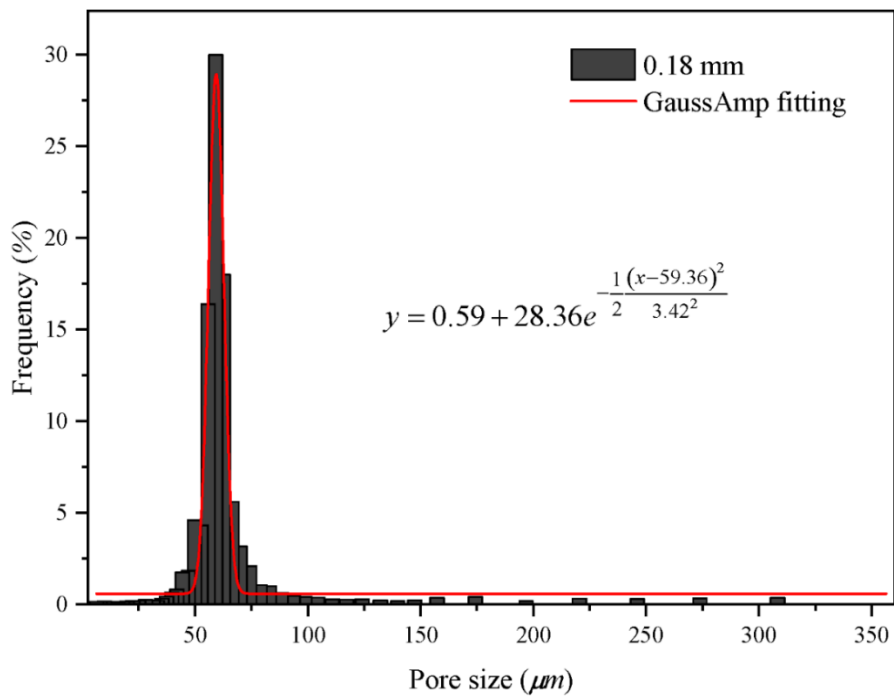
394

395 Figure 9. Histogram of pore size distribution of permeable stone with diameter of 0.36 mm.



396

397 Figure 10. Histogram of pore size distribution of permeable stone with diameter of 0.25 mm.



398

399 Figure 11. Histogram of pore size distribution of permeable stone with diameter of 0.18 mm.

400 From Fig. 8 to Fig. 11 we can find that the pore sizes of the four permeable stones are
 401 uniform and fall within narrow ranges. The pore size distributions of four different particle

402 sizes show a skewed normal distribution. Besides, the pore maximum proportion (the peak of
403 the curve, see Figs. 8-11) of permeable stones with different particle sizes are different, which
404 are 124 μm , 99 μm , 83 μm and 59 μm , respectively. The Gaussian function is widely used to
405 characterize the pore system and classify the petrophysical rock ([Harlan et al., 1995](#); [Jeon et
406 al., 2014](#); [Xu and Torres-Verdín, 2013](#)), and the general form of the Gauss function is shown
407 below:

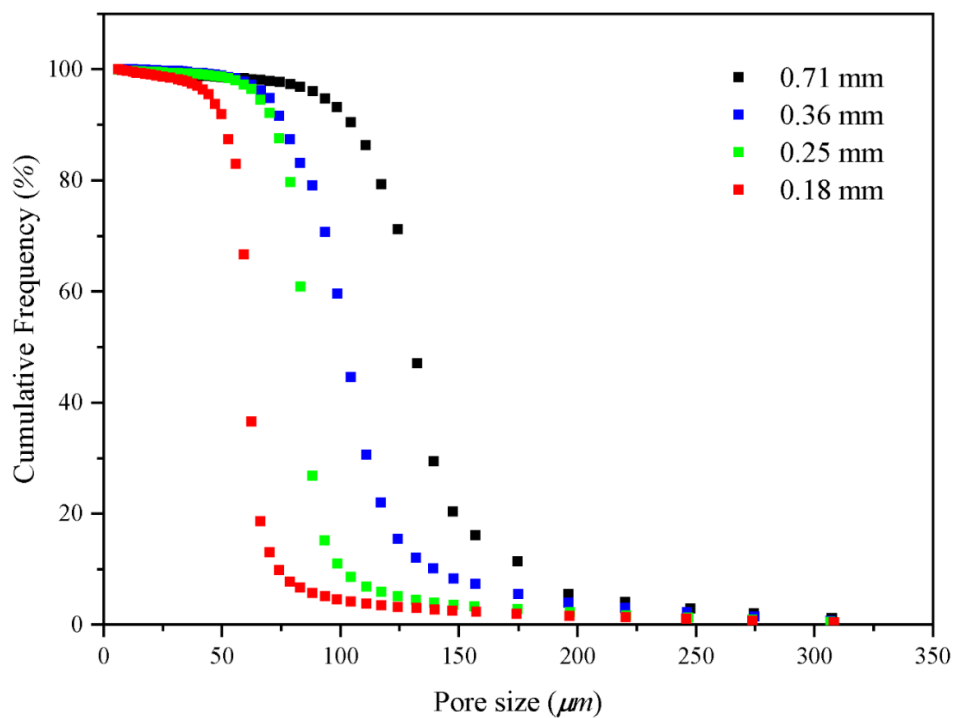
$$y = y_0 + He^{-\frac{(x-x_c)^2}{2w^2}} \quad (3-25)$$

408 where H is the height of the peak of the mercury injection curve, x_c is the abscissa
409 corresponding to the peak of the curve (the pore size), w is the standard variance, which
410 represents the width of the curve. To characterize the distribution of pore structure of four
411 different permeable stones, we best-fit the Gaussian curve of the pore distribution of four
412 permeable stones with different particle sizes, and the best-fitted parameters are shown in
413 Table 2. We can make several interesting observations from Table 2. Firstly, the expected
414 value (x_c) decreases with decreasing particle sizes of permeable stone, and the x_c values of
415 different permeable stones are almost the same. Secondly, the standard variance (w)
416 corresponding to the permeable stone of 0.18 mm is the smallest, indicating that the pore size
417 distribution is more concentrated (or relatively homogeneous). For comparison, the pore size
418 distribution of 0.36 mm permeable stone is the widest with the greatest variance. Finally,
419 different values of H represent different proportions of pore sizes, among which the highest
420 proportion can reach 34.04%. It will be desirable to establish a correlation between the
421 parameters used in the pore-size distribution of Eq. (3-25) with the two Forchheimer
422 coefficients A and B . This objective may be achieved using high-resolution pore-scale fluid
423 mechanics simulations, which are out of the scope of this study. Further research is needed to
424 address this issue in the future.

425 Table 2. Gaussian function characteristic values of four permeable stones with different
 426 particle sizes.

Mesh size	Particle size (mm)	y_0	H	x_c	w
24	0.71	0.73	21.54	127.28	9.00
46	0.36	0.48	13.49	100.48	13.30
60	0.25	0.63	31.88	82.67	4.15
80	0.18	0.59	28.36	59.36	3.42

427 The pore size distributions fall within ever narrower ranges with mesh sizes become
 428 larger. Moreover, the cumulative percentage frequency curves of the pore size distributions
 429 with different particle sizes are exhibited in Fig. 12 and the results are shown in Table 3.



430

431 Figure 12. The cumulative frequency curve of pore size distribution.

432 Fig. 12 shows that DR_{50} (the pore size corresponding to the median pressure P_{50})
 433 increases with the increase of permeable stone particle size, and the mean pore diameter (DR_m)

434 also increases. In general, the pore size corresponding to the median pressure (denoted as
435 \underline{DR}_{50}) may be slightly different than the mean pore diameter (\underline{DR}_m) which has been defined in
436 different ways by various investigators when analyzing the pore size distributions (Hea and
437 Zhangb, 2015; Zhen-Hua et al., 2007; Zhihong et al., 2000). As \underline{DR}_{50} is easily identifiable in
438 the mercury injection experiments, it is used in this study as a representative of the mean pore
439 diameter (\underline{DR}_m) of the permeable stone. Besides, the seepage law of permeable stone is
440 closely related to the pore size, and—the smaller average pore size will result in a larger
441 hydraulic gradient under the condition of the same specific discharge (see Fig. 4). The pore
442 size characteristic values with different particle sizes are listed in Table 3. We find that the
443 porosity decreases as the particle size increases while the mean pore diameter increases. And
444 The mean pore size can reflect the influence of particle diameter, sorting degree and
445 arrangement mode of porous medium on seepage parameters.

446 Table 3. Pore size characteristic values of four permeable stones with different particle sizes.

Mesh size	Porosity (%)	\underline{DR}_m (μm)	\underline{DR}_{50} (μm)
24	32.35	131.31	131.34
46	36.69	102.56	103.42
60	40.82	84.73	85.09
80	42.88	60.97	61.12

447 Note: \underline{DR}_m is the mean pore diameter, \underline{DR}_{50} is the pore diameter corresponding to the median
448 pressure P_{50} .

449 3.3 Analysis of influencing factors of Forchheimer equation coefficients

450 3.3.1 Influence of particle size on equation coefficient

451 The analysis of non-Darcy coefficient has always been of interest to many researchers
 452 working in different disciplines of porous media flow ([Moutsopoulos et al., 2009](#); [Sedghi-Asl](#)
 453 [et al., 2014](#); [Shi et al., 2020](#)). ~~Various studies have suggested expressions for Forchheimer~~
 454 ~~coefficients, different scholars obtained numerous datasets through different experiments and~~
 455 ~~simulation methods to quadratic best fitting the specific discharge hydraulic gradient curves.~~
 456 Different scholars have obtained a large amount of data through different experimental and
 457 simulation methods. They performed a quadratic fitting of the specific discharge and
 458 hydraulic gradient curves, developed numerous expressions for the Forchheimer coefficients.
 459 And We obtained the coefficients of different fitting equations are shown in the following
 460 Table 4.

461 **Table 4.** The Forchheimer coefficients of empirical relations.

Equations	Coefficient A ($\frac{s^2}{m^2sm^{-1}}$)	Coefficient B ($\frac{s^2}{m^2s^2m^{-2}}$)
Ward (1964)	$A = \frac{360}{gd^2}$	$B = \frac{10.44}{gd}$
Blick (1966)	$A = \frac{32}{gnd^2}$	$B = \frac{C_D}{2gn^2d}$
Ergun (1952)	$A = \frac{150(1-n)^2}{gn^3d^2}$	$B = \frac{1.75(1-n)}{gn^3d}$
Macdonald et al. (1979)	$A = \frac{180(1-n)^2}{gn^{3.6}d^2}$	$B = \frac{1.8(1-n)}{gn^{3.6}d}$
Kovács (1981)	$A = \frac{144(1-n)^2}{gn^3d^2}$	$B = \frac{2.4(1-n)}{gn^3d}$
Kadlec and Knight (1996)	$A = \frac{255(1-n)^2}{gn^{3.7}d^2}$	$B = \frac{2(1-n)}{gn^3d}$
Irmay (1964)	$A = \frac{180(1-n)^2}{gn^3d^2}$	$B = \frac{0.6(1-n)}{gn^3d}$

462 [Sidiropoulou et al. \(2007\)](#) focused on the Forchheimer coefficients of porous media and

463 evaluated the original theoretical equation above. The validity of these equations is verified
 464 by using different experimental data. focused on the determination of the Forchheimer
 465 coefficients for non Darcian flow in porous media and evaluated the original theoretical
 466 equations above and the validity of these equations was checked using existing experimental
 467 data. In addition, the Root Mean Square Error (RMSE) was used as a criterion to
 468 quantitatively evaluate the coefficients, ~~and the RMSE was defined as~~

469
$$RMES = \sqrt{\frac{\sum_{i=1}^N (x_i - y_i)^2}{N}}$$
, where x_i were the experimental values of Forchheimer

470 coefficients, y_i were the values computed by different equations above, and N was the total
 471 number of experimental points (Moutsopoulos et al., 2009). The different forms of
 472 Forchheimer coefficients described above are based on different assumptions and
 473 simplifications of pore structure. Consequently, these series of coefficients are applicable
 474 under specific conditions with different degrees of accuracy.

475 According to Eq. (4-2), the hydraulic gradient (J) is composed of a viscous force-related
 476 component (J_n) and an inertia force-related component (J_r), and for detailed discussion of this
 477 matterspecific derivation, please one can refer to previous studies (Huang, 2012):

$$J_n = Aq = \frac{\alpha\mu}{\rho g} \frac{1}{d^2} q \quad J_r = \frac{\beta}{g} \frac{1}{d} q^2 \quad (3-36)$$

478 We can see from Eq. (3-36) that the J_n is inversely proportional to the square of the particle
 479 size, ~~and~~ the J_r is inversely proportional to the particle size when the specific discharge
 480 remains the same. Both J_n and J_r are closely related to specific surface area and sizes of pores.

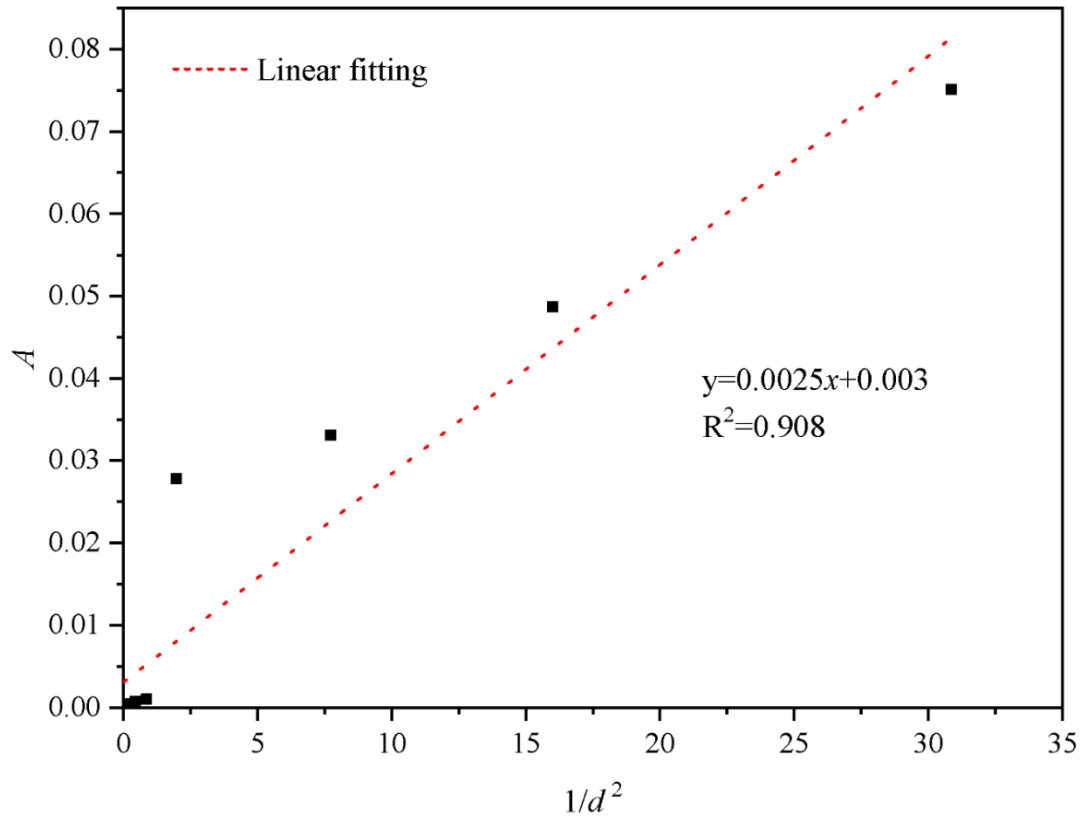
481 As can be seen from the above analysis, the particle size is an important factor affecting the
 482 Forchheimer coefficient. Huang et al. (2013) carried out the seepage experiments in columns
 483 with different particle sizes, including 3mm, 5mm, 8mm and 10mm acrylic spheres.
 484 Therefore, the particle size is an important factor affecting the Forchheimer coefficient,

485 ~~Huang et al. (2013) carried out the experimental investigation on water flow in four columns~~
486 ~~with cubic arrays of acrylic balls in diameter 3 mm, 5 mm, 8 mm and 10 mm, where all the~~
487 ~~acrylic balls are arranged in regular cubes.~~ Accordingly, the coefficients A and B can be
488 written as follows:

$$A = \frac{\alpha \mu}{\rho g} \frac{1}{d^2} \quad B = \frac{\beta}{g} \frac{1}{d} \quad (3-47)$$

489 where α and β are constants related to the shape, sorting, and arrangement of the particles,
490 and the specific derivation process is detailed in the previous study (Huang, 2012). The
491 experimental results showed that the coefficient A was inversely proportional to the particle
492 diameter square (d^2) and coefficient B was inversely proportional to the particle size (d)
493 (Huang et al., 2013).

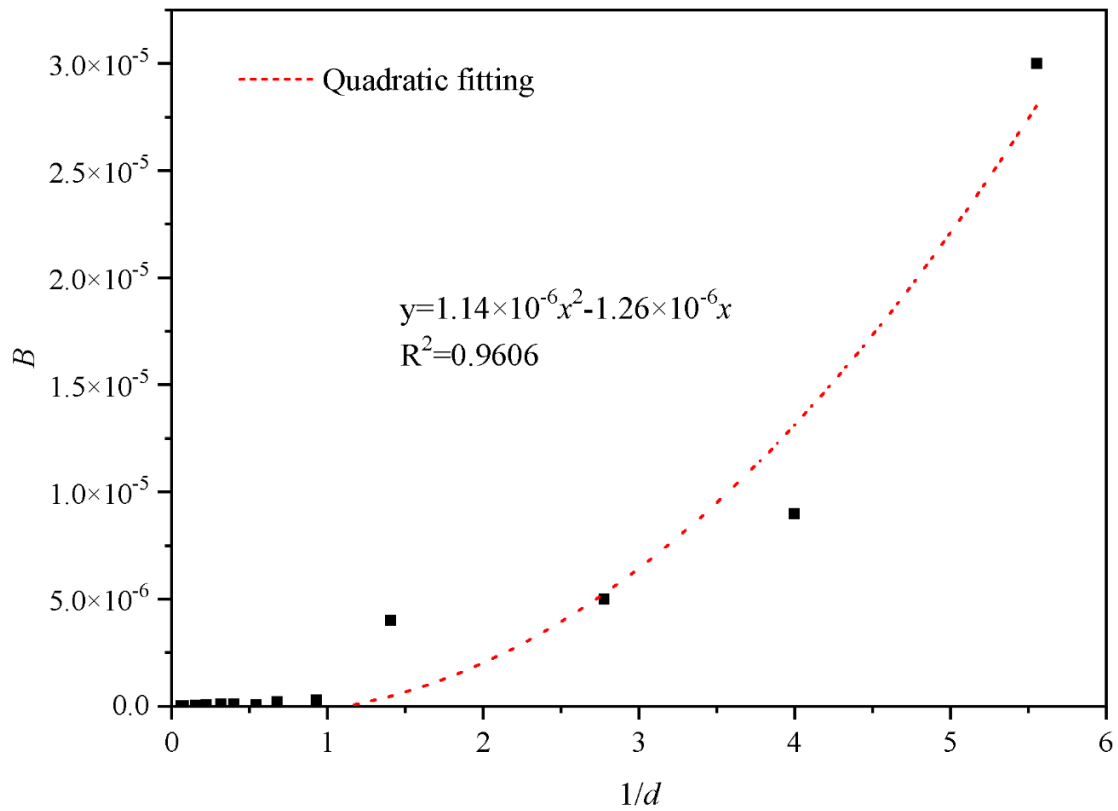
494 The uniform diameter cubic arrangement of porous media mentioned above is a rather
495 ideal medium. The shape and arrangement of particles of natural pore aquifers are usually
496 irregular. Therefore, the above-mentioned linear correlations between A and $1/d^2$, and
497 between B and $1/d$ should be examined specifically. For this purpose, we collect the
498 experimental data of homogeneous porous media, including the previous research results and
499 the results of other scholars. Among them, samples P1-P4 are the permeable stones selected
500 in this study, samples L1-L5 are from previous studies (Li et al., 2017), and the experimental
501 data of samples M1-M4 are from Moutsopoulos et al. (2009). The fitting coefficients are
502 shown in Table 5. Furthermore, we can identify nice correlations between the Forchheimer
503 coefficient A and $1/d^2$ and between the Forchheimer coefficient B and $1/d$, which are shown
504 in Fig. 13 and Fig. 14, respectively.



505

506

Figure 13. Variation of A with $1/d^2$ of different homogeneous particle sizes.



507

508

Figure 14. Variation of B with $1/d$ of different homogeneous particle sizes.

509 We can see from Fig. 13 that the coefficient A is linearly related to $1/d^2$ and the
510 relationship between coefficient A and is given as $A = 0.0025(1/d^2) + 0.003$. ~~And the~~
511 relationship between coefficient B and $1/d$ is completely different from the linear correlation
512 as reported before. Fig. 14 shows that the coefficient B is quadratic related to $1/d$ and the
513 relationship between coefficient B and $1/d$ is given as $B = 1.14 \times 10^{-6} (1/d)^2 - 1.26 \times 10^{-6} (1/d)$.
514 The coefficients A and B show a linear relationship with $1/d^2$ and $1/d$ respectively when the
515 particles are arranged in simple cube arrangement (Huang, 2012). That is to say, the irregular
516 particles such as permeable stones have a more complex geometry, resulting in a different law
517 from that of regular spherical particles. ~~the relationship between coefficient A and $1/d^2$ is~~
518 ~~consistent with the law of simple cubic arrangement porous media, but the relationship~~
519 ~~between coefficient B and $1/d$ is not consistent with the law of simple cubic arrangement~~
520 ~~porous media.~~ The structure of porous medium arranged in cubes is different from the
521 permeable stone. The porosity of the porous media with spheres arranged in cubic is close to
522 0.48, independent of the diameter of spheres. While the particle shape, arrangement and
523 tightness of permeable stone are different, and the porosity of permeable stone with different
524 particle size is also different (see Table 3).

525 Table 5. Experimental fitting coefficient of different homogeneous particle sizes.

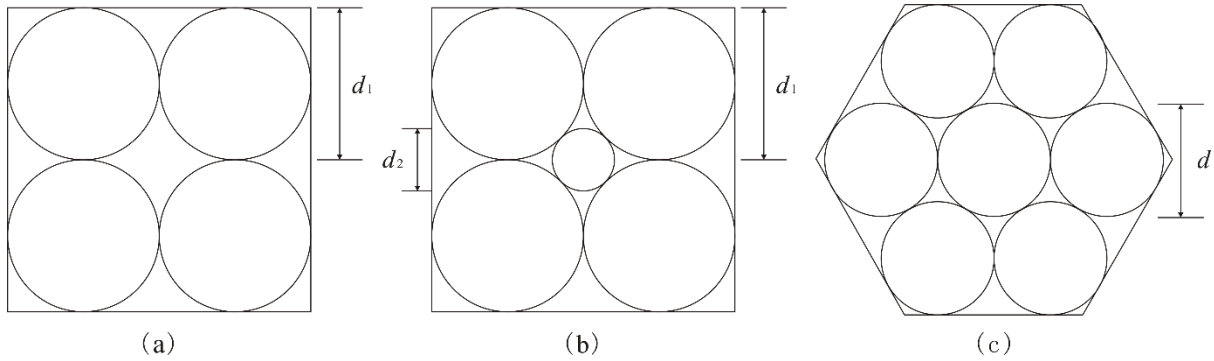
Sample	Particle size (mm)	Fitting equation	A	B	The correlation
P1	0.18	$y = 0.0751x + 3 \times 10^{-5}x^2$	0.0751	3×10^{-5}	0.9995
P2	0.25	$y = 0.0487x + 9 \times 10^{-6}x^2$	0.0487	9×10^{-6}	0.9998
P3	0.36	$y = 0.0331x + 5 \times 10^{-6}x^2$	0.0331	5×10^{-6}	1

P4	0.71	$y=0.0278x+4\times 10^{-6}x^2$	0.0278	4×10^{-6}	0.9995
L1	1.075	$y=0.001x+3\times 10^{-7}x^2$	0.001	3×10^{-7}	0.9999
L2	1.475	$y=0.0007x+2\times 10^{-7}x^2$	0.0007	2×10^{-7}	0.9998
L3	1.85	$y=0.0005x+5\times 10^{-8}x^2$	0.0005	5×10^{-8}	0.9998
L4	2.5	$y=0.0005x+9\times 10^{-8}x^2$	0.0005	9×10^{-8}	0.9997
L5	3.17	$y=0.0004x+1\times 10^{-7}x^2$	0.0004	1×10^{-7}	0.9998
M1	4.5	$y=3\times 10^{-5}x+7\times 10^{-8}x^2$	3×10^{-5}	7×10^{-8}	0.9913
M2	6.39	$y=3\times 10^{-5}x+3\times 10^{-8}x^2$	3×10^{-5}	3×10^{-8}	0.9984
M3	12.84	$y=1\times 10^{-5}x+2\times 10^{-8}x^2$	1×10^{-5}	2×10^{-8}	0.9977
M4	16	$y=1\times 10^{-5}x+2\times 10^{-8}x^2$	1×10^{-5}	2×10^{-8}	0.998

526 3.3.2 Influence of porosity on equation coefficient

527 In above sections, we have analyzed the influence of particle sizes on seepage
528 coefficient. Furthermore, the pore size and pore specific surface area are also related to the
529 arrangement and sorting degree of particles, that is, to the porosity of porous media. To
530 explore the effect of sorting degree on seepage coefficient, we draw a schematic diagram of
531 different sorting degree of particles, as shown in Fig. 15 [\(a\)](#) and [\(b\)](#). The degree of particle
532 sorting is one of the important factors affecting the pore size. In porous media with a poor
533 sorting degree, the pore size is usually determined by the diameter of the smallest particle.
534 We can see from Fig. 15 that the pores between the larger particles are filled by smaller
535 particles, resulting in even smaller pores. In addition, the poorer sorting degree of particles
536 leads to the larger pore specific surface area and stronger viscous force of flow, which can

537 lead to a larger coefficient A .



539 Fig. 15. The schematic diagram of different particle sorting with cube arrangement.

540 Figure 15. The schematic diagram of different particle sizes and arrangements in (a) a cubic
541 arrangement with identical solid grains; (b) a cubic arrangement with two different sizes of
542 solid grains; (c) a hexahedron arrangement with identical solid grains. d_1 is the diameter of
543 (identical) solid grains in (a) and the diameter of the larger solid grains in (b), d_2 is the
544 diameter of the smaller solid grain in (b), d is the diameter of the (identical) solid grains in (c).

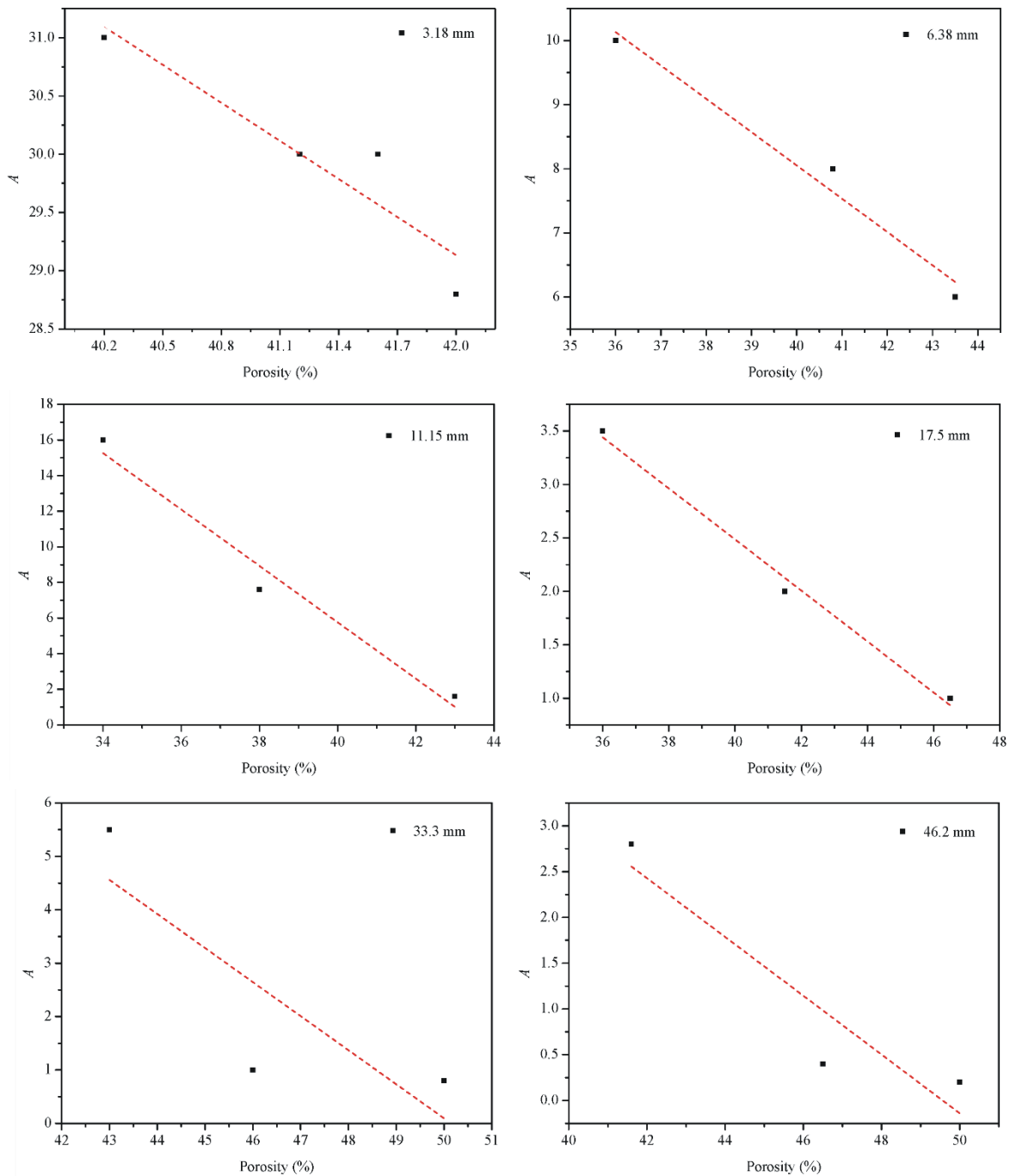
545 Furthermore, we have also provided the schematic diagrams of spherical particles with
546 equal size in two simple arrangements, namely cubic arrangement and hexahedron
547 arrangement, as shown in Fig. 15 (a) and (c). And the cube arrangement is the less
548 compact arrangement with a pore diameter of $0.414d_1$, while the hexahedron arrangement is
549 the more compact arrangement with a pore diameter of $0.155d$, where d_1 and d have been
550 explained in the caption of Fig. 15. The characteristic value of pore structure in different
551 arrangement with the same particle size are shown in Table 6. We can see that different
552 arrangement modes will substantially affect the pore specific surface area and pore size of
553 porous media. The more compactly packed particles lead to the larger pore specific surface
554 area and stronger viscous force. Meanwhile, the smaller pore diameter is associated with
555 stronger effect of viscous force and inertia force. In summary, the better sorting degree of
556 particles leads to the weaker viscous and inertial forces, then the coefficients A and B will be

557 smaller. As the better sorting degree and the less compact (or looser) arrangement particles
558 mean the larger porosity, so we can conclude that the larger porosity leads to the smaller
559 coefficients A and B under the condition of the same particle size.

560 Table 6. Characteristic value of pore structure in different arrangement with the same particle
561 size.

Arrangement mode	Side length	Porosity (%)	Specific surface area
Cube	$2d$	47.60	3.142
Hexahedron	$1.577d$	43.30	3.402

562 However, the structure of natural porous media is much more complex and
563 heterogeneous than what has been shown in Figure [4615](#), so it is difficult to quantitatively
564 describe the effect of sorting degree and arrangement on seepage law.



565

566

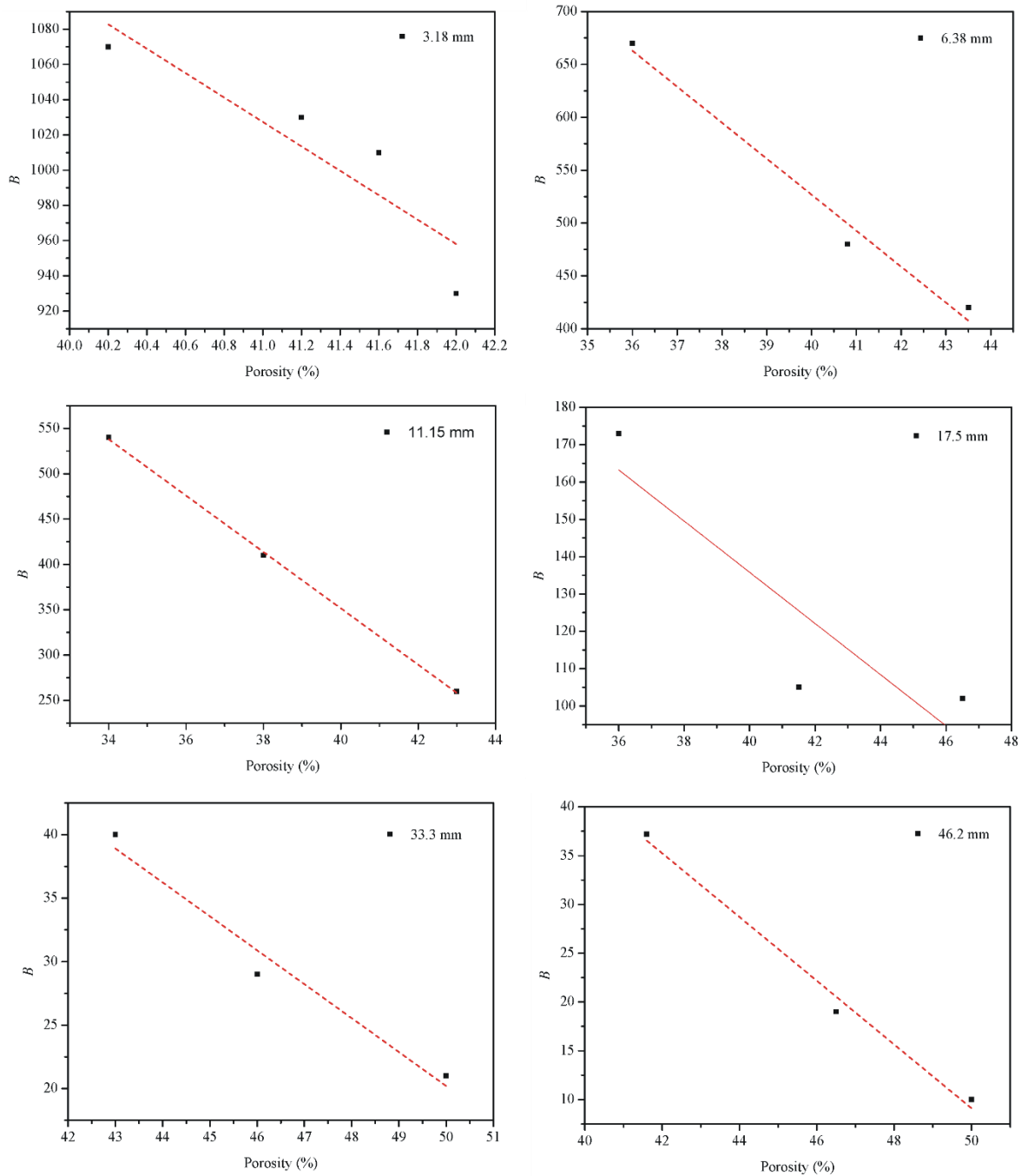
Figure 4716. Variation of A with n of six gravels with different particle sizes.

567

In view of this, we can use a macro parameter porosity (n) to reveal the effect of sorting degree and arrangement on seepage coefficient. In order to verify the correctness of the above analysis results, we selected the seepage experiment results of [Niranjan \(1973\)](#) for further validation. [Niranjan \(1973\)](#) chose gravel of the same size but different porosity and carried out seepage experiments. We selected the experimental results of six different particle sizes

571

572 with 3.18 mm, 6.38 mm, 11.15 mm, 17.5 mm, 33.3 mm and 46.2 mm from [Niranjan \(1973\)](#),
 573 and drew the relationship between coefficient A and B and porosity respectively, as shown in
 574 Fig. [17-16](#) and Fig. [18-17](#). We can see that the coefficients A and B of the six groups of
 575 experimental data of [Niranjan \(1973\)](#) decrease with the increase of porosity, which is
 576 consistent with our theoretical analysis of this investigation.



577

578 Figure [18-17](#). Variation of B with n of six gravels with different particle sizes.

579 4. Summary and conclusions

580 This study presents experimental results of Forchheimer flow in four different
581 permeable stones with different mesh sizes, including 24 mesh size (0.71 mm), 46 mesh size
582 (0.36 mm), 60 mesh size (0.25 mm), 80 mesh size (0.18 mm). The effects of mean pore size
583 and pore size distribution on the transition of flow regimes (from pre-~~Darcian~~Darcy to post-
584 ~~Darcian~~Darcy) are discussed. In addition, the mercury injection ~~technique experiment~~ is
585 proposed to investigate the pore distribution of the permeable stones. ~~Beyond that~~ In addition,
586 the Forchheimer coefficients are specifically discussed. The main conclusions can be
587 summarized as follows:

588 1) The relationships between specific discharge (q) and the “pseudo” hydraulic conductivity
589 (K) (which is computed as a ratio of q and the hydraulic gradient, J) of permeable stones
590 show that deviation from ~~Darcian flow~~Darcy flow regime is clearly visible. In addition, the
591 critical specific discharge corresponding to the transition of flow regimes (from pre-
592 ~~Darcian~~Darcy to post-~~Darcian~~Darcy) increases with the increase of mean particle size.

593 2) When the specific discharge is small, only a small fraction of the pore water flowing
594 through the pores. The rest of the pore water adheres to the surface of the solid particles
595 (immobile), partially blocking the flow pathways. As the specific discharge increases, more
596 pore water becomes mobile and participates in flow. Hence, the "pseudo" hydraulic
597 conductivity increases with the increase of specific discharge. When the specific discharge
598 increases to the critical specific discharge (q_c), the "pseudo" hydraulic conductivity is
599 maximized, and then it begins to decrease as the specific discharge continues to increase.

600 3) The mercury injection experiment results show that the mercury injection curve can be
601 divided into three segments. The beginning and end segments of the mercury injection curve
602 of the four permeable stones with different particle sizes are very gentle, while the main (or
603 intermediate) mercury injection curve is steep, indicating that the pore size distribution falls

604 within a narrow range, ~~and~~ the proportions of large pores and small pores are relatively small.

605 4) The porosity decreases as the mean particle size of permeable stone increases while the

606 mean pore diameter increases. ~~And~~ ~~t~~ The porosity can reflect the influence of particle

607 diameter, sorting degree and arrangement mode of porous medium on seepage parameters.

608 ~~The~~ ~~A~~ larger porosity leads to ~~the~~ smaller coefficients A and B under the condition of the

609 same particle size.

610 5) The coefficient A is linearly related to $1/d^2$ and the relationship between coefficient A and

611 $1/d^2$ is given as $A = 0.0025(1/d^2) + 0.003$. The coefficient B is not linearly related to $1/d$,

612 instead it is quadratic related to $1/d$ as $B = 1.14 \times 10^{-6} (1/d)^2 - 1.26 \times 10^{-6} (1/d)$. The particle

613 shape and arrangement of permeable stone have imposed great influences on the seepage

614 parameters.

615 **Notation**

616 q The specific discharge, $\text{md}^{-1}\text{m/d}$.

617 K The “pseudo” hydraulic conductivity, md^{-1} .

618 J The dimensionless parameter defined as hydraulic gradient.

619 A The Forchheimer equation coefficient (viscous force item), sm^{-1} .

620 B The Forchheimer equation coefficient (Inertia force item), s^2m^{-2} .

621 a, b The empirical parameters depend on materials properties.

622 Re The Reynold number.

623 Re_c The critical Reynold number.

624 M, m The coefficients determined by fluid and properties.

625 C_D The appropriate phenomenological coefficient.

626 P_c The capillary force, Pa .

627	P_{50}	The corresponding pressure value when the saturation reaches 50%, <i>MPa</i> .
628	P_A, P_B, P_C	The pressure corresponding to different stages on mercury injection curve, <i>MPa</i> .
629	σ	The solid-liquid interfacial tension, <i>Nm⁻¹</i> .
630	θ	The wet angle between the liquid and the solid surface.
631	r	The radius of curvature in capillary, <i>mm</i> .
632	d	The particle size, <i>mm</i> .
633	d_{50}	The mean particle sizes (50% by weight), <i>mm</i> .
634	D_m	The mean pore diameter, μm .
635	D_{50}	The pore diameter corresponding to the median pressure P_{50} , μm .
636	H	The height of the peak of the mercury injection curve.
637	x_c	The abscissa corresponding to the peak of the curve (the pore size).
638	w	The standard variance.
639	n	The porosity.
640	J_n	The viscous force-related component.
641	J_r	The inertia force-related component.

642 **Authors contributions**

643 Zhongxia Li: Experiment, Writing original draft. Junwei Wan: Methodology,
644 Conceptualization. Tao Xiong: Data curation, Investigation, Experiment. Hongbin Zhan:
645 Methodology, Writing, Review & Editing. Linqing He: Experiment, Methodology. Kun
646 Huang: Funding acquisition, Investigation

647 **Competing interests**

648 The authors declare that they have no conflict of interest.

649 **Acknowledgements**

650 This study was supported by the National Natural Science Foundation of China (Grant
651 Nos. 41402204), the National Key Research and Development Program of China
652 (No. 2018YFC0604202) and the Fundamental Research Funds for National Universities,
653 China University of Geosciences (Wuhan). Thank Zhongzhi Shen of China University of
654 Geosciences for his great help in developing the experimental set up. ~~The And the~~ authors
655 want to express their sincere appreciation of the constructive comments made by the two
656 anonymous reviewers and Associate Editor for improving the quality of the manuscript.

657 **References**

- 658 Alvarez, A. E., Mahmoud, E., Martin, A. E., Masad, E., and Estakhri, C.: Stone-on-stone contact of permeable
659 friction course mixtures, *Journal of Materials in Civil Engineering*, 22, 1129-1138,
660 [https://doi.org/10.1061/\(ASCE\)MT.1943-5533.0000117](https://doi.org/10.1061/(ASCE)MT.1943-5533.0000117), 2010.
- 661 Anovitz, L. M. and Cole, D. R.: Characterization and Analysis of Porosity and Pore Structures, *Reviews in*
662 *Mineralogy and Geochemistry*, 80, 61-164, <https://doi.org/10.2138/rmg.2015.80.04>, 2015.
- 663 Bear, J.: *Dynamics of Fluids in Porous Media*, American Elsevier Pub. Co., New York, N.Y., and
664 Amsterdam, 1972.
- 665 Beavers, G. S., Sparrow, E., and Rodenz, D. E.: Influence of Bed Size on the Flow Characteristics and Porosity
666 of Randomly Packed Beds of Spheres, *Journal of Applied Mechanics*, 40, 655-660,
667 <https://doi.org/10.1115/1.3423067>, 1972.
- 668 Blick, E.: Capillary-Orifice Model for High-Speed Flow through Porous Media, *Industrial Engineering*
669 *Chemistry Process Design Development*, 5, 90-94, <https://doi.org/10.1021/i260017a019>, 1966.
- 670 Bu, S., Yang, J., Dong, Q., and Wang, Q.: Experimental study of transition flow in packed beds of spheres with
671 different particle sizes based on electrochemical microelectrodes measurement, *Applied Thermal Engineering*,
672 73, 1525-1532, 2014.
- 673 Darcy, H.: *Recherches expérimentales relatives au mouvement de l'eau dans les tuyaux*, Impr. Impériale, Paris,
674 France, 1857.
- 675 Dejam, M., Hassanzadeh, H., and Chen, Z.: Pre-Darcy flow in porous media, *Water Resources Research*, 53,
676 8187-8210, <https://doi.org/10.1002/2017WR021257>, 2017.
- 677 Dudgeon, C. R.: An experimental study of the flow of water through coarse granular media, *La Houille Blanche*,
678 785-801, <https://doi.org/10.1051/lhb/1966049>, 1966.
- 679 Dybbs, A. and Edwards, R.: A new look at porous media fluid mechanics—Darcy to turbulent, in: *Fundamentals*
680 *of transport phenomena in porous media*, Springer, 199-256, 1984.

681 Ergun, S.: Fluid flow through packed columns, Chemical Engineering Progress, 89-94,
682 [https://doi.org/10.1016/0009-2509\(53\)80048-5](https://doi.org/10.1016/0009-2509(53)80048-5), 1952.

683 Fancher, G. H. and Lewis, J. A.: Flow of simple fluids through porous materials, Industrial & Engineering
684 Chemistry, 25, 1139-1147, <https://doi.org/10.1021/ie50286a020>, 1933.

685 Fetter, C. W.: Applied Hydrogeology: International Edition, Prentice Hall, Pearson, Englewood Cliffs, 2001.

686 Forchheimer, P.: Wasserbewegung durch boden, Z. Ver. Deutsch, Ing., 45, 1728-1782, 1901.

687 Geertsma, J.: Estimating the Coefficient of Inertial Resistance in Fluid Flow Through Porous Media, Society of
688 Petroleum Engineers Journal, 14, 445-450, <https://doi.org/10.2118/4706-PA>, 1974.

689 Guan, X., Wang, J., and Xiao, F.: Sponge city strategy and application of pavement materials in sponge city,
690 Journal of Cleaner Production, 127022, <https://doi.org/10.1016/j.jclepro.2021.127022>, 2021.

691 Hall, P. L., Mildner, D., and Borst, R. L.: Small-angle scattering studies of the pore spaces of shaly rocks,
692 Journal of Geophysical Research Atmospheres, 91, 2183-2192, <https://doi.org/10.1029/JB091iB02p02183>, 1986.

693 Han, D., Wei, L., and Zhang, J.: Experimental study on performance of asphalt mixture designed by different
694 method, Procedia engineering, 137, 407-414, <https://doi.org/10.1016/j.proeng.2016.01.275>, 2016.

695 Harlan, J., Picot, D., Loll, P., and Garavito, R.: Calibration of size-exclusion chromatography: use of a double
696 Gaussian distribution function to describe pore sizes, Analytical biochemistry, 224, 557-563,
697 <https://doi.org/10.1006/abio.1995.1087>, 1995.

698 Hea, X. and Zhangb, Z.: Microscopic Pore Structural Characteristics in Coal Particles, International Conference
699 on Material, Guangzhou, China,

700 Huang, K.: Exploration of the basic seepage equation in porous media, PhD dissertation, 2012.

701 Huang, K., Wan, J., Chen, C., Linqing, H., Mei, W., and Zhang, M.: Experimental investigation on water flow in
702 cubic arrays of spheres, Journal of Hydrology, 492, 61-68, <https://doi.org/10.1016/j.jhydro.2013.03.039>, 2013.

703 Irmay, S.: Theoretical models of flow through porous media, RILEM Symp. Transfer of Water in porous media,
704 Paris, Bull. RILEM, 29, 37-43, 1964.

705 Izbash, S.: O Filtracii V Kropnozernstom Materiale, Leningrad, USSR, 1931.

706 Javadi, M., Sharifzadeh, M., Shahriar, K., and Mitani, Y.: Critical Reynolds number for nonlinear flow through
707 rough walled fractures: The role of shear processes, Water Resources Research, 50, 1789-1804,
708 <https://doi.org/10.1002/2013WR014610>, 2014.

709 Jeon, H., Cho, H., Kim, J., and Sung, B.: Non-Gaussian rotational diffusion in heterogeneous media, Physical
710 Review E Statistical Nonlinear & Soft Matter Physics, 90, 042105, <https://doi.org/10.1103/PhysRevE.90.042105>,
711 2014.

712 Kadlec, R. H. and Knight, R. L.: Treatment Wetlands, Lewis Pub, Boca Raton, 1996.

713 Kate, J. M. and Gokhale, C. S.: A simple method to estimate complete pore size distribution of rocks,
714 Engineering Geology, 84, 48-69, <https://doi.org/10.1016/j.enggeo.2005.11.009>, 2006.

715 Koch, D. and Ladd, A.: Moderate Reynolds number flows through periodic and random arrays of aligned
716 cylinders, Journal of Fluid Mechanics, 349, 31-66, <https://doi.org/10.1017/S002211209700671X>, 1996.

717 Kovács, G.: Seepage Hydraulics, Development in Water Sciences. Elsevier: New York, 1981.

718 Latifi, M., Midoux, N., Storck, A., and Gence, J.: The use of micro-electrodes in the study of the flow regimes in
719 a packed bed reactor with single phase liquid flow, Chemical engineering science, 44, 2501-2508, 1989.

720 Li, Q., Wang, F., Yu, Y., Huang, Z., Li, M., and Guan, Y. J. J. o. E. M.: Comprehensive performance evaluation
721 of LID practices for the sponge city construction: a case study in Guangxi, China, Journal of Environmental
722 Management, 231, 10-20, <https://doi.org/10.1016/j.jenvman.2018.10.024>, 2019a.

723 Li, Z., Wan, J., Huang, K., Chang, W., and He, Y.: Effects of particle diameter on flow characteristics in sand
724 columns, *International Journal of Heat & Mass Transfer*, 104, 533-536,
725 <https://doi.org/10.1016/j.ijheatmasstransfer.2016.08.085>, 2017.

726 Li, Z., Wan, J., Zhan, H., Cheng, X., Chang, W., and Huang, K.: Particle size distribution on Forchheimer flow
727 and transition of flow regimes in porous media, *Journal of Hydrology*, 574, 1-11,
728 <https://doi.org/10.1016/j.jhydrol.2019.04.026>, 2019b.

729 Lindquist, E.: On the flow of water through porous soil, Premier Congres des grands barrages (Stockholm)1933.

730 Lindquist, W. B., Venkatarangan, A., Dunsmuir, J., and Wong, T. F.: Pore and throat size distributions measured
731 from synchrotron X-ray tomographic images of Fontainebleau sandstones, *Journal of Geophysical Research*
732 *Solid Earth*, 105, 21509-21527, <https://doi.org/10.1029/2000JB900208>, 2000.

733 Maakal, O., Prat, M., Peinador, R., and Lasseux, D.: Determination of the throat size distribution of a porous
734 medium as an inverse optimization problem combining pore network modeling and genetic and hill climbing
735 algorithms, *Physical Review E*, 103, 023303, <https://doi.org/10.1103/PhysRevE.103.023303>, 2021.

736 Macdonald, I., El-Sayed, M., Mow, K., and Dullien, F.: Flow through porous media -the Ergun equation revisited,
737 *Industrial & Engineering Chemistry Fundamentals*, 18, 199-208, <https://doi.org/10.1021/i160071a001>, 1979.

738 Moutsopoulos, K. N., Papaspyros, I. N., and Tsihrintzis, V. A.: Experimental investigation of inertial flow
739 processes in porous media, *Journal of hydrology*, 374, 242-254, <https://doi.org/10.1016/j.jhydrol.2009.06.015>,
740 2009.

741 Niranjana, H.: Non-Darcy flow through porous media, M.S., dissertation, ITT, Kanpur, India, 1973.

742 Panfilov, M. and Fourar, M.: Physical splitting of nonlinear effects in high-velocity stable flow through porous
743 media, *Advances in Water Resources*, 29, 30-41, <https://doi.org/10.1016/j.advwatres.2005.05.002>, 2006.

744 Pittman, E. D.: Relationship of porosity and permeability to various parameters derived from mercury injection -
745 capillary pressure curves for sandstone (1), AAPG bulletin, 76, 191-198, [https://doi.org/10.1306/BDF87A4-
746 1718-11D7-8645000102C1865D](https://doi.org/10.1306/BDF87A4-1718-11D7-8645000102C1865D), 1992.

747 Prowell, B. D., Allen Cooley Jr, L., and Schreck, R. J.: Virginia's experience with 9.5-mm nominal-maximum-
748 aggregate-size stone matrix asphalt, *Transportation research record*, 1813, 133-141,
749 <https://doi.org/10.3141/1813-16>, 2002.

750 Rezaee, R., Saeedi, A., and Clennell, B.: Tight gas sands permeability estimation from mercury injection
751 capillary pressure and nuclear magnetic resonance data, *Journal of Petroleum Science and Engineering*, 88, 92-
752 99, <https://doi.org/10.1016/j.petrol.2011.12.014>, 2012.

753 Rijfkogel, L. S., Ghanbarian, B., Hu, Q., and Liu, H. H.: Clarifying pore diameter, pore width, and their
754 relationship through pressure measurements: A critical study, *Marine and Petroleum Geology*, 107, 142-148,
755 <https://doi.org/10.1016/j.marpetgeo.2019.05.019>, 2019.

756 Scheidegger, A.: The physics of flow through porous media,
757 Scheidegger, A. E.: On the stability of displacement fronts in porous media: a discussion of the muskat-
758 aronofsky model, *Canadian Journal of Physics*, 38, 153-162, <https://doi.org/10.1139/p60-017>, 1960.

759 Scheidegger, A. E.: The physics of flow through porous media, University of Toronto Press,
760 <https://doi.org/10.3138/9781487583750>, 2020.

761 Schmitt, M., Fernandes, C. P., da Cunha Neto, J. A., Wolf, F. G., and dos Santos, V. S.: Characterization of pore
762 systems in seal rocks using nitrogen gas adsorption combined with mercury injection capillary pressure
763 techniques, *Marine and Petroleum Geology*, 39, 138-149, <https://doi.org/10.1016/j.marpetgeo.2012.09.001>, 2013.

764 Schneebeli, G.: Experiences sur la limite de validite de la loi de Darcy et l'apparition de la turbulence dans un

765 ecoulemant de filtration, *La Huille Blanche*, 2, 141-149, <https://doi.org/10.1051/lhb/1955030>, 1955.

766 Sedghi-Asl, M., Rahimi, H., and Salehi, R.: Non-Darcy Flow of Water Through a Packed Column Test,
767 *Transport in Porous Media*, 101, 215-227, <https://doi.org/10.1007/s11242-013-0240-0>, 2014.

768 Seguin, D., Montillet, A., Comiti, J., and Huet, F.: Experimental characterization of flow regimes in various
769 porous media—II: Transition to turbulent regime, *Chemical engineering science*, 53, 3897-3909, 1998.

770 Shi, W., Yang, T., and Yu, S.: Experimental Investigation on Non-Darcy Flow Behavior of Granular Limestone
771 with Different Porosity, *Journal of Hydrologic Engineering*, 25, 06020004,
772 [https://doi.org/10.1061/\(ASCE\)HE.1943-5584.0001966](https://doi.org/10.1061/(ASCE)HE.1943-5584.0001966), 2020.

773 Sidiropoulou, M. G., Moutsopoulos, K. N., and Tsihrintzis, V.: Determination of Forchheimer equation
774 coefficients a and b, *Hydrological Processes*, 21, 534-554, <https://doi.org/10.1002/hyp.6264>, 2007.

775 Skjetne, E., Hansen, A., and Gudmundsson, J.: High-velocity flow in a rough fracture, *Journal of Fluid
776 Mechanics*, 383, 1-28, <https://doi.org/10.1017/S0022112098002444>, 1999.

777 Soni, J., Islam, N., and Basak, P.: An experimental evaluation of non-Darcian flow in porous media, *Journal of
778 Hydrology*, 38, 231-241, [https://doi.org/10.1016/0022-1694\(78\)90070-7](https://doi.org/10.1016/0022-1694(78)90070-7), 1978.

779 Souto, H. P. A. and Moyne, C.: Dispersion in two-dimensional periodic porous media. Part I. Hydrodynamics,
780 *Physics of Fluids*, 9, 2243-2252, <https://doi.org/10.1063/1.869365>, 1997.

781 Suo, Z., Bao, X., Nie, L., Yan, Q., and Qi, K.: Optimization Design of Mix Proportion of Large Stone Permeable
782 Mixture Based on Target Air Voids, *Buildings*, 11, 514, <https://doi.org/10.3390/buildings11110514>, 2021.

783 Swartzendruber, D.: Modification of Darcy's law for the flow of water in soils, *Soil Science*, 93, 22-29,
784 <https://doi.org/10.1097/00010694-196201000-00005>, 1962a.

785 Swartzendruber, D.: Non-Darcy flow behavior in liquid-saturated porous media, *Journal of Geophysical
786 Research*, 67, 5205-5213, <https://doi.org/10.1029/JZ067i013p05205>, 1962b.

787 Van Lopik, J. H., Zazai, L., Hartog, N., and Schotting, R.: Nonlinear Flow Behavior in Packed Beds of Natural
788 and Variably Graded Granular Materials, *Transport in Porous Media*, 131, 957-983,
789 <https://doi.org/10.1007/s11242-019-01373-0>, 2019.

790 Van Lopik, J. H., Snoeijers, R., van Dooren, T. C. G. W., Raoof, A., and Schotting, R. J.: The Effect of Grain
791 Size Distribution on Nonlinear Flow Behavior in Sandy Porous Media, *Transport in Porous Media*, 120, 1-30,
792 <https://doi.org/10.1007/s11242-017-0903-3>, 2017.

793 Wang, J., Ng, P.-L., Gong, Y., Su, H., and Du, J.: Experimental Study of Low Temperature Performance of
794 Porous Asphalt Mixture, *Applied Sciences*, 11, 4029, <https://doi.org/10.3390/app11094029>, 2021.

795 Ward, J. C.: Turbulent Flow in Porous Media, *Journal of Hydraulic Engineering*, 90, 1-12,
796 [http://dx.doi.org/10.1016/S0301-9322\(02\)00051-4](http://dx.doi.org/10.1016/S0301-9322(02)00051-4), 1964.

797 Washburn, E. W.: The Dynamics of Capillary Flow, *Physical Review*, 17, 273-283,
798 <https://doi.org/10.1103/PhysRev.17.273>, 1921.

799 Wright, D.: Nonlinear Flow Through Granular Media, *Journal of Hydraulic Engineering*, 94, 851-872,
800 <https://doi.org/10.1061/JYCEAJ.0001858>, 1968.

801 Xie, H. and Watson, D. E.: Determining air voids content of compacted stone matrix asphalt mixtures,
802 *Transportation research record*, 1891, 203-211, <https://doi.org/10.3141/1891-24>, 2004.

803 Xu, C. and Torres-Verdín, C.: Pore System Characterization and Petrophysical Rock Classification Using a
804 Bimodal Gaussian Density Function, *Mathematical Geosciences*, 45, 753-771, [https://doi.org/10.1007/s11004-](https://doi.org/10.1007/s11004-013-9473-2)
805 [013-9473-2](https://doi.org/10.1007/s11004-013-9473-2), 2013.

806 Yang, B., Yang, T., Xu, Z., Liu, H., Yang, X., and Shi, W.: Impact of Particle-Size Distribution on Flow

807 Properties of a Packed Column, *Journal of Hydrologic Engineering*, 24, 04018070,
808 [https://doi.org/10.1061/\(ASCE\)HE.1943-5584.0001735](https://doi.org/10.1061/(ASCE)HE.1943-5584.0001735), 2019.

809 Yu, T., Liu, D., Zhang, H., and Wang, H.: Influence of pore water phase change on service performance for
810 permeable pavement in Sponge City, *Water Science and Technology*, 84, 3769-3779,
811 <https://doi.org/10.2166/wst.2021.459>, 2021.

812 Zeng, Z. and Grigg, R.: A criterion for non-Darcy flow in porous media, *Transport in porous media*, 63, 57-69,
813 <https://doi.org/10.1007/s11242-005-2720-3>, 2006.

814 Zhen-hua, MIN, and, Min, CAO, and, Shu, ZHANG, and, and Xiu-dan: Effect of precursor on the pore structure
815 of carbon foams, *New Carbon Materials*, 22, 75-79, [https://doi.org/10.1016/S1872-5805\(07\)60009-2](https://doi.org/10.1016/S1872-5805(07)60009-2), 2007.

816 Zhihong, L. I., Jihong, S., Dong, W. U., Yuhua, S., Liu, Y. I., Wenjun, S., and Baozhong, D.: Determination of
817 average pore diameter of SiO₂ xerogels by small angle X-ray scattering, *ACTA Physica sinica*, 49, 1312-1315,
818 <https://doi.org/10.3321/j.issn:1000-3290.2000.07.020>, 2000.

819 Zhou, H., Fang, Y.-g., Chen, M., Gu, R.-g., and Li, W.: Experimental and analytical study on electro-osmosis in
820 low-permeability soil considering the pore size effect, *Geotechnique*, 71, 141-152,
821 <https://doi.org/10.1680/jgeot.18.p.362>, 2019.

822